SkinPlot:

A Programmable Thin and Soft Skin-drag Display Using Shape Memory Alloys

Master's Thesis
submitted to the
Media Computing Group
Prof. Dr. Jan Borchers
Computer Science Department
RWTH Aachen University

by
Moritz Messerschmidt

Thesis advisor:
Prof. Dr. Jan Borchers

Second examiner:
Prof. Dr. Stefan Kowalewski

Registration date: 24.09.2019
Submission date: 19.12.2019

Eidesstattliche Versicherung

______________________________ ______________________________

Name, Vorname   Matrikelnummer

Ich versichere hiermit an Eides Statt, dass ich die vorliegende Arbeit/Bachelorarbeit/ Masterarbeit* mit dem Titel

____

____

____

selbständig und ohne unzulässige fremde Hilfe erbracht habe. Ich habe keine anderen als die angegebenen Quellen und Hilfsmittel benutzt. Für den Fall, dass die Arbeit zusätzlich auf einem Datenträger eingereicht wird, erkläre ich, dass die schriftliche und die elektronische Form vollständig übereinstimmen. Die Arbeit hat in gleicher oder ähnlicher Form noch keiner Prüfungsbehörde vorgelegen.

______________________________ ______________________________

Ort, Datum   Unterschrift

*Nichtzutreffendes bitte streichen

Belehrung:

§ 156 StGB: Falsche Versicherung an Eides Statt

Wer vor einer zur Abnahme einer Versicherung an Eides Statt zuständigen Behörde eine solche Versicherung falsch abgibt oder unter Berufung auf eine solche Versicherung falsch aussagt, wird mit Freiheitsstrafe bis zu drei Jahren oder mit Geldstrafe bestraft.

§ 161 StGB: Fahrlässiger Falscheid; fahrlässige falsche Versicherung an Eides Statt

(1) Wenn eine der in den §§ 154 bis 156 bezeichneten Handlungen aus Fahrlässigkeit begangen worden ist, so tritt Freiheitsstrafe bis zu einem Jahr oder Geldstrafe ein.

(2) Straflosigkeit tritt ein, wenn der Täter die falsche Angabe rechtzeitig berichtigt. Die Vorschriften des § 158 Abs. 2 und 3 gelten entsprechend.

Die vorstehende Belehrung habe ich zur Kenntnis genommen:

______________________________ ______________________________

Ort, Datum   Unterschrift

Contents

Abstract **xvii**

Acknowledgements **xix**

Conventions **xxi**

1 Introduction **1**

1.1 Outline 3

2 Related work **5**

2.1 Haptic Interfaces Using Conventional Actuators 5

2.2 Towards Unobtrusive Wearable Tactile Displays 7

2.2.1 Tactile Output Using Shape-Memory Alloys 8

2.3 Natural and Expressive Skin-drag Gestures . 10

3 Design and Implementation Concepts of Shape-Memory Alloys **13**

3.1 Shape-Memory Alloys as Design Material . . . 14
3.1.1 Types of Shape-Memory Alloys 14
Shape-Memory Effect 14
Activation Stimulus 15
3.2 Shape-memory Alloy Actuators 15
3.2.1 Nickel-Titanium SMAs 16
Electro-mechanical Implemenation . . 17
3.2.2 Actuator Characteristics 17
3.2.3 Form Factors 19
3.3 Basic Spring Actuator Implementation 20
3.3.1 Physical Design Parameters 20
3.3.2 Control Parameters 21
3.3.3 Basic Control of a Contraction 23
3.3.4 Repeated Contractions 24
Contraction Frequency 26
Active vs. Passive Configuration Test 26
3.3.5 Closed Loop Control 28
Self Sensing Test 28
3.4 Advanced Spring Actuator Control and Implementation Concepts 30
3.4.1 Topologies 30
3.4.2 Connecting Multiple SMA Actuators 31

3.4.3 Controlling Multiple Nodes 32

Half-bridge Output Control 33

3.4.4 Body Grounding 35

3.4.5 Generic Controller Board 35

4 Skin-drag Display 37

4.1 Display Design 37

4.2 Control Model 39

4.2.1 Force Equilibrium Model 41

Discussion 42

4.2.2 Boosted Movements Model 42

Discussion 45

4.2.3 Hybrid Model 46

Discussion 47

4.3 Implementation 48

4.3.1 Display 48

4.3.2 Control System 50

4.3.3 Machine Controller Interface 51

Gesture Definition 51

Command Interface 52

System State and Feedback 53

5 Design Tool 55

5.1 Design Tool Components 55

5.1.1 Shadow Movements 57

5.1.2 Cool Down 57

5.2 Gesture Design 58

5.2.1 Defining the Movement Path 58

5.2.2 Time and Speed Control 59

5.3 Plotting a Gesture 59

6 Evaluation **61**

6.1 Technical Evaluation 61

6.1.1 Apparatus and Setup 62

6.1.2 Design and Procedure 63

Target Acquisition Task 63

Sequence of Movements Task 64

6.1.3 Measurements 65

6.1.4 Results and Discussion 66

Individual Target Acquisitions 66

Sequences of Target Acquisitions . . . 68

6.1.5 Conclusion 69

6.2 On-Skin Perception 71

6.2.1 Setup 72

6.2.2 Gesture Selection 72

6.2.3 Design and Procedure 72

6.2.4 Participants 74

6.2.5 Results and Observations 75

Overall Results 75

Shape Related Results 76

Speed Related Results 77

6.2.6 Observations and Discussion 77

6.2.7 Conclusion 79

6.3 Design Tool Usability 80

6.3.1 Setup 80

6.3.2 Design and Procedure 81

6.3.3 Results and Observations 82

Shape Matching 82

UI Components 83

6.3.4 Conclusion 84

7 Summary and future work **85**

7.1 Summary and contributions 85

7.2 Limitations and Future Work 87

7.2.1 Skin-drag Display 87

7.2.2 Control Unit 89

A Generic Spring Controller Board Schematic **91**

B Skin-drag Display Control Circuit Schematic 93

C Time-Distance-Power Relation 95

D Perception Study Questionnaires 97

E Usability Study Questionnaires 101

Bibliography 105

Acronyms 115

Index 117

List of Figures

2.1 Conventional Actuators for Haptic Feedback 6

2.2 Tactile Displays using SMAs 9

2.3 Conventional Actuators vs. SMA Soft Actuators for Multimodal On-Skin Sensations . . 10

2.4 Skin-drag Sensations 11

2.5 Skin-drag Displays 12

3.1 NiTi Thermal One-way Shape-memory Effect 16

3.2 Typical Temperature to Strain Characteristics of NiTi SMA Wires 18

3.3 SMA Spring Design Parameters 21

3.4 Basic Spring Actuator Control 23

3.5 Gate Driver Schematic 24

3.6 SMA Spring with Bias Spring 25

3.7 Active Bias Spring Configuration 27

3.8 SMA Spring Resistance vs. Displacement . . 29

3.9 Different Topologies 30

3.10 SMA Mesh Prototype 31
3.11 Half-bridge Schematic 34
3.12 SMA Controller Board 36

4.1 4-Star Topology Design Parameters 38
4.2 EMA Comparison 39
4.3 Force Equilibrium Model 41
4.4 Time-Distance-Power Relationship 44
4.5 Force Ratio 45
4.6 Hybrid Model Phases 46
4.7 2D Actuator Assembly 48
4.8 Gate Driver Schematic 49
4.9 Control Circuit Breadboard 50
4.10 Sequence of Movements 52

5.1 Gesture Design Tool 56

6.1 Technical Evaluation Top View 62
6.2 Technical Evaluation Target Points 63
6.3 Technical Evaluation Shapes 64
6.4 Target Acquisition Error Comparison 66
6.5 Systematic Error 67
6.6 Technical Evaluation Plotted Shapes 68
6.7 Cooling Deformation Effect 70

6.8 User Study Hand Mount 71
6.9 Shape Confusion and Subjective Rating . . . 75
6.10 Noticeability and Confidence by Shape . . . 76
6.11 Noticeability and Confidence by Speed . . . 77
6.12 Design Task Rating 83

7.1 Shrinking the System Size 87
7.2 Gliding Plate and Tactor Control 88

A.1 Generic Spring Controller Board Schematic . 92

B.1 Skin-drag Display Control Circuit Schematic 94

D.1 Perception Study Questionnaire Trials (1) . . 97
D.2 Perception Study Questionnaire Trials (2) . . 98
D.3 Perception Study Questionnaire Trials (3) . . 99
D.4 Perception Study Questionnaire Overall . . . 100

E.1 Usability Study Questionnaire Trials 102
E.2 Usability Study Questionnaire Overall . . . 103

List of Tables

3.1 Thermal One-way SMA Actuator Characteristics 20

3.2 Half-bridge Output Logic 34

4.1 Command Interface 53

6.1 Shape Targeting Errors 69

Abstract

Wearable interfaces offer a yet rarely exploited potential for addressing our sense of touch through always available haptic feedback in mobile scenarios. So far, conventional systems primarily rely on vibro-tactile cues to convey discrete information and deliver meaningful feedback when our visual and auditory perception is distracted or being unavailable. Vibration, however, only depicts one of many tactile stimuli we perceive through our skin and the majority of proposed wearable devices still reveal to be rigid and bulky. Recent advances in material science brought about new soft actuators and smart materials which reveal promising characteristics in order to provide more natural and expressive feedback modalities through unobtrusive wearable interfaces.

Within this thesis we investigate on the implementation and control of shape-memory alloy (SMA) spring actuators for on-skin applications. Based on our initial tests, we present a first proof-of-concept of a thin and soft skin-drag display which takes advantage of the high force-to-weight ratio, smooth operation and large displacement length of the flexible actuators. Our prototype implements a star topology of four antagonistic SMA springs which affords to plot two-dimensional skin-drag gestures according to a simple and robust control model. A separately developed design tool allows to program our device in an easy way and test diverse gestures leveraging the high perceptibility of skin-drag sensations. Our system targets researchers who seek to explore two-dimensional skin-drag gestures which offer to convey information in an intuitive way through the skin for various application scenarios.

The proposed system is evaluated in a technical way regarding accuracy and consistency of repeated target acquisitions as well as the performance of plotting different shapes. Next to our technical evaluation we conducted a preliminary user study within which we investigated on the perceptibility of the developed prototype and the usability of our design tool.

Acknowledgements

First of all, I would like to thank my thesis advisor Prof. Dr. Jan Borchers for supporting me and providing me with the opportunity to write my master's thesis at the Media Computing Group. In addition, I would like to thank Prof. Dr. Stefan Kowalewski for examining my thesis as second examiner.

I would like to thank Nur Al-Huda Hamdan and Adrian Wagner for supervising me and allowing me to follow my passion for haptics in the field of HCI by working on this topic. It was an exciting experience to work under your supervision. While you provided me with valuable feedback and expertise during our meetings, our conversations have always been characterized by amusing and open-minded discussions about new – sometimes crazy – ideas.

I also want to thank all the participants who volunteered for my user studies and spent their time on providing me with helpful feedback.

Finally, I want to say thanks to my friends and my family who offered me a comfortable environment while I was working on this thesis.

Conventions

Throughout this thesis we use the following conventions.

The whole thesis is written in American English. The first person is written in the plural form. Any participant will be referred to by using the pronoun 'she'.

Important phrases and technical terms are emphasized using *italics*. Marginal notes aim to summarize key points.

Definitions of technical terms or short excursus are set off in coloured boxes.

EXCURSUS:
Excursus are detailed discussions of a particular point in a book, usually in an appendix, or digressions in a written text.

Definition: *Excursus*

Chapter 1

Introduction

Our sense of touch is one of the most important senses we use to perceive our world and interact with the environment. Aside from our visual and auditory perception, it offers a unique information channel which allows to provide expressive feedback in a discreet way. Since researchers discovered that certain types of mechanoreceptors are very sensitive to external vibration stimuli [Sato 1961; Gray and Matthews 1951], vibratory feedback has primarily been suggested to communicate through the skin [Geldard 1960]. As vibration motors are cheap and can be obtained in small sized form factors, they have mainly been considered for mobile applications during the past decades [Tan and Pentland 1997; Lee and Starner 2009; Luzhnica and Veas 2019]. Vibration, however, only depicts one of many ways to provide tactile information through our skin. Next to vibration, our mechanoreceptors have shown to be sensitive to a variety of other tactile stimuli such as brush, pressure, stretch and motion [Delmas et al. 2011].

With the recent trend of mobile computing and a growing demand for a realistic experience in virtual reality environments, more expressive tactile feedback through unobtrusive wearable devices has become increasingly relevant. Several work has proposed more natural feedback modalities by producing different stimuli and mimicking typical human-to-human gestures, such as squeezing, dragging and tapping [Caswell et al. 2012; Stanley and Kuchenbecker 2011]. The intuitive gestures can be understood immediately and do not require prior training by the user. The majority of the proposed devices, however, relies on conventional actuators including electric motors, solenoids and hydraulic pumps. The actuators introduce bulkiness, rigidity and noisy mechanisms which are inappropriate for preferably unobtrusive wearable interfaces.

Due to the advances in material science, new soft actuators and smart materials are getting available for researchers. With the help of the new technology, they are able to develop thinner and more flexible devices that provide a higher degree of wearability. Recently, Hamdan et al. [2019] showed how shape-memory alloy (SMA) actuators can be implemented for on-skin applications by designing thin and flexible stickers that are able to mimic different natural gestures. However, the stickers so far can only generate a limited range of natural gestures. Once the actuators are attached to the skin, pulling, stretching or dragging can mainly be performed in one dimension. Previous work has proposed using a conventional actuation system to drag a tactor across the skin and perform two-dimensional skin-drag gestures [Ion et al. 2015]. This type of feedback system has the potential to replay a variety of different gestures which are appropriate for diverse application scenarios.

We therefore intended to built a programmable two-dimensional skin-drag display using SMAs that is able to retain a high degree of wearability and can mimic a variety of different natural feeling gestures. To provide researchers with a toolkit to explore diverse skin-drag gestures we furthermore aimed to develop a design tool which allows to program our device in an easy way.

Working towards a programmable and unobtrusive wearable interface using SMAs that allows to replay various skin-drag gestures in two dimensions, this thesis seeks to contribute in mainly four ways: (1) We present a first proof-of-concept of a thin and soft skin-drag display which uses a star topology of four SMA spring actuators. (2) We show how we can realize a simple but robust control model thanks to the antagonistic configuration of the implemented soft actuators. (3) Our control circuit is able to drive four spring actuators according to our control model such that gestures can be performed by instructing a machine controller using a command interface. (4) We developed a software design tool which aims to provide researchers with the ability to explore diverse skin-drag gestures and program our skin-drag display in an intuitive way.

1.1 Outline

In the following chapter (chapter 2), we discuss and compare so far proposed wearable haptic feedback devices. We show up how SMAs have been considered in the field of human-computer interaction (HCI) by now and mention the benefit of using SMA spring actuators in context of wearable skin-drag displays.

In chapter 3, we discuss the control and implementation of SMA *spring actuators* which show to have rarely been considered for on-skin applications so far. This chapter in particular aims to share our experiences from our initially conducted tests.

Within chapter 4, we present the design of our skin-drag display using SMAs and elaborate on how we establish a simplified control system which allows to plot two-dimensional gestures according to our developed control model.

While chapter 4 focuses on the implementation of the backend, we subsequently show how one can easily program the proposed skin-drag display and design gestures in an intuitive way using our developed design tool (chapter 5). We discuss how the different UI components aim to convey the limitations and boundaries of our developed display.

Finally, we evaluate our device in a technical way and discuss the results of our preliminary user study which focuses on the perceptibility of our device as well as the usability of the proposed design tool (chapter 6). We conclude by summarizing our work, discussing so far existing limitations, and showing up potential starting points for future work in chapter 7.

Chapter 2

Related work

Several work has focused on providing more expressive and natural tactile feedback beyond vibration. In the following, we will show up how researchers aim to provide other kinds of *tactile feedback modalities* for various *application scenarios* by proposing different *actuation systems* for wearable interfaces. Subsequently, we discuss so far existing interfaces based on shape-memory alloy actuators and elaborate on how these may enhance skin-drag displays which still show to rely on conventional actuators.

2.1 Haptic Interfaces Using Conventional Actuators

There have been several attempts to provide more expressive and natural tactile feedback modalities for wearable interfaces using conventional actuators. The approaches implement electric motors, piezoelectric actuators, electrodes, selenoids, ultrasonic technology or even pneumatic and hydraulic actuators in order to produce soft as well as very strong sensations (Figure 2.1).

Stanley and Kuchenbecker [2011] presented multiple wearable tactile actuators based on servo motors to reproduce common human to human gestures at the forearm. With

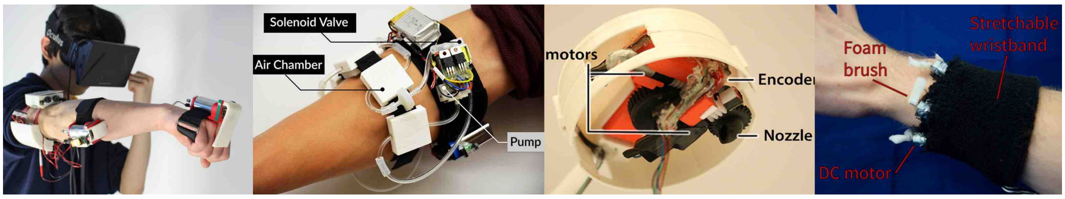

Figure 2.1: Conventional actuators for haptic feedback (left to right): 'Impacto' push, pressure and impact sensations using electric stimulation and solenoids [Lopes et al. 2015a]; 'PneuHaptic' soft squeezing and pressure sensations using inflatable airchambers [He et al. 2015]; 'Jetto' directional push and pressure using a controlled air stream [Gong et al. 2018]; 'BrushTouch' brush sensations using electric motors [Strasnick et al. 2017].

Electric motors and solenoids belong to most conventional actuators, but unveil to be heavy, thick and stiff. Their implementation often introduces noisy mechanisms causing unwanted vibrations.

'BrushTouch' Strasnick et al. [2017] produce soft but easily noticeable brushing sensations by attaching rotary motors at a wearable wristband (Figure 2.1). Je et al. [2017] presented 'tactoRing', a fingerworn DC-motor driven interface which provides discrete notifications through skin-dragging gestures. Also Tsai et al. [2019] recently showcased a prototype which embeds traditional rotary motors as well as movement brakes for more realistic elastic force feedback within Virtual Reality (VR) environments. In a similar manner Lopes et al. [2015b] combined solenoids and electric stimulation to provide more immersive impact stimuli for VR applications (Figure 2.1). 'MagTics' demonstrated several implementation- and fabrication concepts for electromagnetic actuators, yielding in more flexible and realistic on-body applications which provide tactile feedback across the fingers and the hand palm [Pece et al. 2017]. Recently, Mcintosh et al. [2019] proposed on-body and around-the-device interaction techniques using solenoids and a magnet worn at the fingertip for tactile feedback including pressure and vibration.

Ultrasonic technology allows for miniaturized arrays of pins or invoking sensations through acoustic waves, but they still remain rigid and limited to pressure stimuli.

Kim et al. [2009] and Jin et al. [2014] offered prototypes using piezoelectric tiny ultrasonic linear actuators (TULAs) for grounded as well as forearm worn tactile displays involving arrays of pins for generating textures or providing spatial cues through invoked pressure stimuli. Spelmezan et al. [2016] considered an apparatus which uses acoustic ultrasound transmitters and an corresponding receiver being directly attached to the skin in order to produce focused pressure or vibration stimuli with 'SkinHaptics'.

Gong et al. [2018] presented a novel pneumatic system called ’Jetto’ which uses an adjustable air stream nozzle to provide directional cues and lateral force feedback for emulating impact and pushing gestures; they demonstrate to enhance video- and gaming experiences for mobile devices like smart-watches (Figure 2.1). With ’PneuHaptic’ He et al. [2015] reveal a pneumatic system offering more gentle squeezing and pressure sensations through inflatable air chambers incorporated in a wearable armband. Han et al. [2018] revealed a compelling thin finger worn ’Hydroring’ which is capable of addressing ’pressure, vibration and temperature’ stimuli for mixed-reality applications.

Hydraulic and pneumatic systems require pipes, pumps, and bulky air cartridges.

While the proposed devices offer novel ways to augment our tactile perception for mobile interaction scenarios by invoking different sensations, they show to be limited regarding their form factor, rigidity and complex setup. Their thickness and bulkiness primarily reveals to be introduced by the integrated solenoids, pumps and rotary motors which furthermore comprise noisy mechanical components. Pneumatic and hydraulic systems require pipes, valves, compressed air cartridges or fluids; they thus still encompass cumbersome actuation mechanisms which appear to be inappropriate in order to design preferably unobtrusive wearable interfaces.

2.2 Towards Unobtrusive Wearable Tactile Displays

Tacttoo

[Withana et al. 2018]

Next to very thin and flexible layers of electrodes which provide tactile output using electric stimulation [Withana et al. 2018], especially soft actuators based on smart materials have shown to provide compelling alternatives to traditional actuators during the past years. Koo et al. [2008] developed a thin layer of dielectric elastomer actuators (DEAs) which provide mechanical pressure on the skin. The system, however, requires very high activation voltages (up to $3.5kV$). Chossat et al. [2019] recently used twisted and coiled polymer (TCP) actuators to produce lateral skin-stretch stimuli at the index finger using lower voltages. Nevertheless, the authors report that the actuator still requires $60V$ to generate a contraction of 5.2% of the actuators relaxed length.

Electro stimulation is limited to pressure and vibration stimuli; DEAs require very high voltages for actuation.

Recently, shape-memory alloy actuators arose great interest for on-body applications. The cheap soft actuators offer a simple implementation while remaining noiseless and flexible. They offer a high force-to-weight ratio and provide a displacement length of $5-50\%$ depending on their form factor. Compared to dielectric polymer actuators, they require relatively low activation voltages within a safe range of $3-9V$ which is provided by common power supplies and batteries [DYNALLOY Inc. 2019; TOKI Corporation 2017].

2.2.1 Tactile Output Using Shape-Memory Alloys

Only recently, SMAs have increasingly been considered for on-body applications.

The utilization of shape-memory alloys as soft actuator has been explored excessively in various application domains during the past decades [Mohd Jani et al. 2014]; though, few wearable on-skin devices have been proposed in the field of HCI so far [Qamar et al. 2018]. Prior work in particular presented non-wearable interfaces using the high contraction force, but low recovery strain of SMA wires for creating visually organic and tactile brushing experiences [Coelho and Maes 2008; Probst et al. 2011; Nojima et al. 2013; Ooide et al. 2013; Nakayasu 2016]. Due to the smooth behavior of the soft actuators they have also been considered for on-the-go scenarios, by means of enhancing social interaction through shape changing mobile devices or wearable textiles [Coelho et al. 2008; Park et al. 2015; Lin et al. 2015; Duvall et al. 2016].

The approaches mainly focus on mimicking basic gestures by using SMA actuators.

Only few work has proposed using the soft actuators for on-skin tactile feedback applications which focus on more expressive sensations within diverse contexts (Figure 2.2). Scheibe et al. [2007] presented a first on-skin tactile display for virtual reality environments by providing pressure stimuli through direct contact of SMA wires at the fingertips. Solazzi et al. [2011] proposed a first 2-DoF tactile skin-

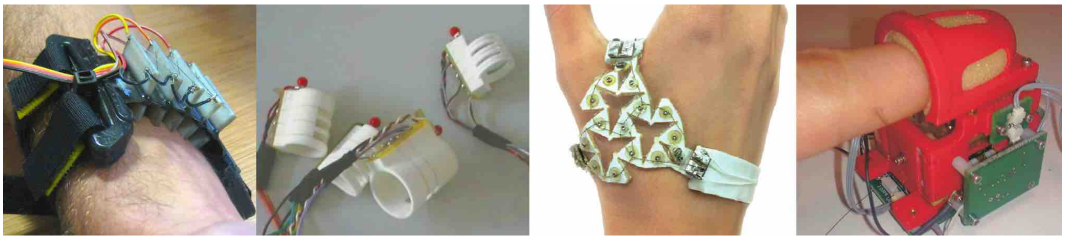

Figure 2.2: Tactile Displays using SMAs (left to right): 'The Tickler' stroking gesture at the forearm [Knoop and Rossiter 2015]; Pressure cues at the fingertips for VR environments [Scheibe et al. 2007]; 'Skin+' stronger touch sensation through an auxetic structure at the back of the hand [Cao et al. 2018]; 2-DoF skin stretch at the fingertips [Solazzi et al. 2011].

drag device for the finger tip, providing directional cues by moving a tactor up to $2mm$ in each direction; the system however still remains rigid and bulky, and does not show to take advantage of the promising thin and flexible properties of shape-memory alloys. In contrast, Cao et al. [2018] proposed a thin back of the hand 'visuo-tactile interface' that translates the low displacement length of SMA wires into stronger touch sensations by using an auxetic structure. In a similar fashion 'The Tickler' uses several bars which generate 'natural-feeling' stroking gestures upon the contraction of interconnected SMA wires [Knoop and Rossiter 2015]. Gupta et al. [2017] investigated on producing squeezing sensations using the contraction of individual SMA spring actuators which are implemented in a wristband. Recently, Hamdan et al. [2019] showed how to fabricate small on-skin stickers which implement SMA spring actuators in order to produce a variety of sensations. The authors take advantage of the up to ten times larger displacement length of the actuators and demonstrate how they mimic natural gestures such as pinching, stretching and dragging. The wearable stickers especially unveil to outperform traditional actuators due to their simplicity and being able to provide tactile feedback at so far challenging on-body locations thanks to their their small sized form factor and flexibility (see Figure 2.3).

SMA actuators offer promising characteristics for on-body applications and provide a compelling alternative to conventional actuators.

The systems show that SMA actuators provide a compelling alternative to traditional actuators and produce expressive tactile feedback. However, they only cover a limited subset of primitive

Figure 2.3: Four wristband worn actuators for natural human to human gestures using conventional servo motors [Stanley and Kuchenbecker 2011] (left); Six 'Springlets' stickers for expressive natural gestures using SMA spring actuators [Hamdan et al. 2019] (right). The thin and flexible soft actuators allow for more challenging on-skin locations while offering strong and silent sensations at the same time.

natural gestures and reveal to primarily rely on a binary or coarse control of the soft actuators. Dragging and stretching of the skin is mainly performed in one dimension or addresses a comparable low skin area. Hence, the systems appear to be mostly suited for providing basic (directional) cues.

2.3 Natural and Expressive Skin-drag Gestures

Skin-drag displays offer expressive feedback through natural and intuitive gestures for different contexts.

In contrast, skin-drag displays which drag a tactor across the skin aim to exploit the spatial dimension and offer to replay a range of distinct natural-feeling gestures which are applicable for a variety of different applications. Despite vibro-tactile feedback is conventionally preferred for encoding information, the vibration stimuli on its own tends to be abstract and feel artificial. Skin-drag gestures instead, combine pressure, stretch and vibration by dragging an object across the skin and stimulating different types of mechanoreceptors (Figure 2.4). This way they are able to invoke comparable strong sensations [Ion et al. 2015] and

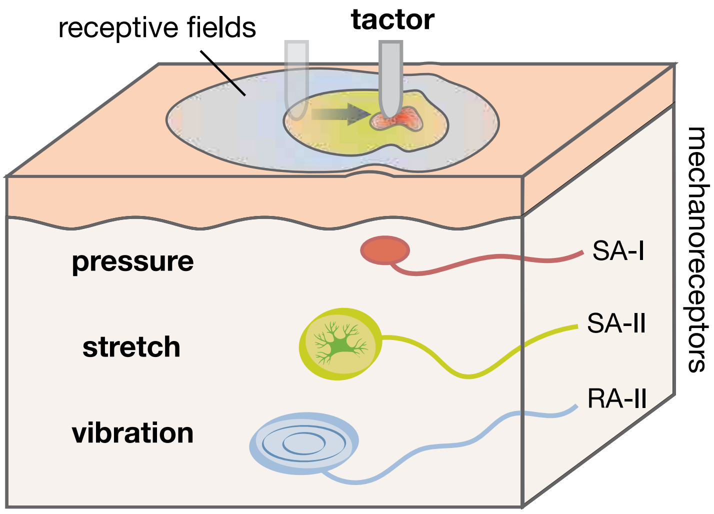

Figure 2.4: A physical tactor which is dragged across the skin surface, stimulates different types of mechanoreceptors being sensitive to pressure, stretch and vibration stimuli within their respective receptive fields. The illustration is inspired by Ion et al. [2015] and Delmas et al. [2011].

generate natural feeling gestures which can be understood immediately; they thus do not require prior training by the user.

Ion et al. [2015] showed that people are good in perceiving skin-drag gestures within a relatively small skin area at the forearm. They claim that their skin-drag display outperforms a vibro-tactile display enclosing the same skin region regarding geometric shapes. Je et al. [2017] presented 'TactoRing', a wearable tactile display which drags a physical tactor around the finger. They found that users could distinguish eight distinct points around the finger through movements performed relative to a homing position. Caswell et al. [2012] developed a self-contained wearable skin-stretch device which suggests a directional discrimination threshold below $2mm$.

Skin-dragging can provide strong sensations within a small skin area by combining multiple stimuli.

Also other work report a 'remarkable' ability of recognizing directional cues at the forearm and back of the hand [Olausson et al. 1998; Olausson 1994; Edin 1992], skin-drag

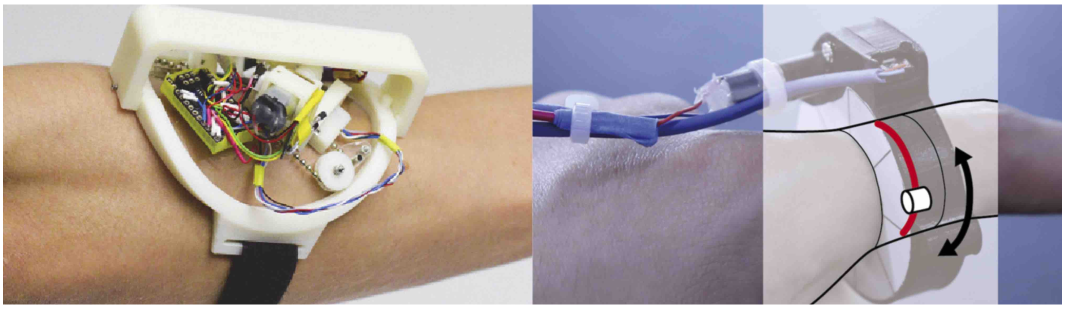

Figure 2.5: Two wearable skin-drag displays: Ion et al. [2015] plot geometric shapes at the forearm (left); the 'tactoRing' drag a tactor around the finger [Je et al. 2017] (right). The systems are able to perform highly perceptible gestures within a small skin area; though they remain rigid and noisy by implementing conventional actuators which introduce unwanted vibrations and noise.

Unwanted distortions introduced by a wearable system should be minimized to unleash the high directional perceptibly of our skin.

displays can potentially benefit from. However, Olausson et al. [2000] state that especially the directional discriminability of a movable tactor on the skin can be sensible to 'disturbances of the somatosensory system'. Hence, other disturbing factors introduced by the wearable system itself, such as unwanted vibrations, should be minimized.

The so far proposed skin-drag devices still rely on electrical motors and unveil to be stiff and bulky (see Figure 2.5). They furthermore show to be prone to cause unwanted pressure and vibration which can distort our sensory system.

SMA actuators could provide a thin and flexible actuation mechanism for providing soft and smooth skin-drag gestures.

We therefore aimed to take advantage of the thin and flexible properties of SMA actuators and design a soft skin-drag display which offers a smooth motion system. The device should this way allow to replay two-dimensional gestures by dragging an object across the skin and comprise a first step towards an unobtrusive wearable skin-drag device. To enable researchers to investigate on the supported skin-drag gestures, we furthermore wanted to provide a tool which allows to program our system in an easy way.

Chapter 3

Design and Implementation Concepts of Shape-Memory Alloys

Utilizing shape-memory alloy (SMA) springs for on-skin applications has rarely been explored so far. The aim of this chapter is to summarize the experience gathered through our initial tests which lead to the design decisions for our prototype described in chapter 4. It moreover serves as introduction to shape-memory alloys as design material in general and gives a basic understanding on how SMA springs may be implemented as actuator for on-skin applications.

In the following, we will briefly show up which types of SMAs exist, describe their main characteristics, and thereby motivate our decision of using SMA spring actuators for our application. We will furthermore discuss general approaches of controlling SMA springs and introduce several implementation concepts along with the common terminology which serves as foundation for the subsequent chapters.

3.1 Shape-Memory Alloys as Design Material

SMAs belong to the category of smart materials which exhibit a so called shape-memory effect (SME). The ability to 'memorize' a certain shape constitutes the key characteristic of this kind of material. As SMAs can be designed to recover a previously specified shape under certain conditions, they are particularly suitable to form very thin actuators for small scaled mechanisms. When they change from one shape to another, they generate force and movement which can be used for actuation. As the raw material by itself is not limited to a certain form factor and the 'memorized' shape may be programmed to meet the individual needs, it is being used in a variety of different domains, such as robotics, biomedical and automotive applications [Mohd Jani et al. 2014].

3.1.1 Types of Shape-Memory Alloys

There exist different types of SMAs which offer their own unique properties making them more or less suitable for certain applications. SMAs primarily differ by the *type of SME* they exhibit and the *stimulus* they react to.

Shape-Memory Effect

SMAs can exhibit a *one-way* or a *two-way* shape-memory effect and either react to a *thermal* or a *magnetic* stimulus.

SMAs either have a *one-way SME* or a *two-way SME* [Motzki 2018]. SMAs with a *one-way SME* restore a memorized shape when stimulated and retain the shape after stimulation. To restore the initial shape, an external force is required. In contrast, a *two-way SME* allows the material to shift between two 'memorized' shapes. Hence, when a *two-way SMA* is stimulated, it transforms to a memeorized shape; and once the stimulus is removed, the SMA returns to another memorized shape without the need for an external force. Consequently, a *two-way SMA* can generate force and movement during both transformations. Although, a *two-way SME* may appear superior to a *one-way SME*, it is not necessarily preferable for many applications as the material introduces stiffness and thus suffers from less flexibility. They furthermore have shown to be less reliable for long term usage involving repeated activation cycles [Sun et al. 2012].

Activation Stimulus

The shape change of an SMA usually can be induced upon the exposure of two different stimuli: a *magnetic field* (magnetic SME) or *heat* (thermal SME). The composition of the metal alloy defines to which degree an SMA reacts to either of them. SMAs specifically designed to react to one of the stimuli are therefore called *thermal SMA* or *magnetic SMA*. The latter is also known as ferromagnetic shape-memory alloy (FSMA). A major drawback of FSMAs is that they usually require a relatively strong magnetic field which cannot be induced by the material itself and consequently requires additional external components. As thermal SMAs can take advantage of the *Jule heating effect* (3.2.1), they are often better suited for small actuator implementations.

3.2 Shape-memory Alloy Actuators

SMA actuators are designed to exploit the SME of an SMA by maximizing the generated physical force or displacement upon actuation. Throughout this thesis, we will solely refer to nickel-titanium (NiTi) SMA actuators with a *thermal one-way SME*. This type of alloy has shown to provide most reliable characteristics for long-term operations. Thus it is predominantly used by manufacturers to produce SMA actuators which allow for a high number of repeated actuation cycles [Cederström and Van Humbeeck 1995]. The *one-way SME* of NiTi SMAs is preferred over a *two-way SME* as it allows for a deformation of the material when not being excited. This is interesting for a large range of applications which can this way take advantage of the actuator's flexibility. As a consequence, the SMA actuators only provide

From now on we will refer to NiTi SMA actuators with a thermal one-way SME. The used actuators contract upon actuation.

force and movement in one way. The SMA actuators we use, are especially designed to contract by a certain fraction of their length and thereby generate a *contraction force*. To allow for repeated contractions the actuators have to be elongated again. We discuss different techniques which allow for repeated contractions later on in subsection 3.3.4.

3.2.1 Nickel-Titanium SMAs

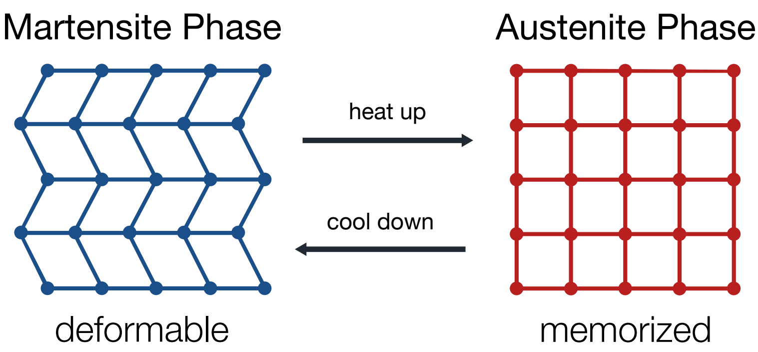

Figure 3.1: Simplified illustration of the thermal *one-way shape-memory effect* of NiTi alloys: At low temperature the *martensite phase* allows to deform the material. When heated up the inner crystalline structure enters the *austenite phase*; restoring the deformation and allowing to recover a 'preprogrammed' shape.

At low temperature the smart material remains flexible, by heating it up the inner crystalline structure transforms and thereby restores a memorized shape.

The unique characteristics of NiTi alloys rely on its inner structure which allows switching between two crystalline forms on a microscopic scale (Figure 3.1). Depending on the temperature level and internally caused stress, the material undergoes a phase transformation between the *martensite* and *austenite* phase. The temperature thresholds for the individual but not necessarily distinct phases are commonly referred to as the *austenite start temperature* A_s and *austenite finish temperature* A_f; as well as the corresponding start and finish temperature thresholds for the *martensite phase* M_s and M_f. The finish temperatures, here, describe the extremes (M_f low temperature, A_f high temperature) at which the material is considered to fully take on either of the forms. At low temperature ($M_f \leq T \leq M_s$) the inner crystalline structure takes on its *martensite* form at which the material remains flexible and can be deformed on macroscopic scale. At high temperature ($A_s \leq T \leq A_f$) the internally caused stress forces the crystalline structure to take on its *austenite* form. During this transformation the material becomes stiff and can thereby restore a 'memorized' shape on macroscopic scale. The temperature thresholds for the phases vary among the differently manufactured metal alloys. Most NiTi SMA actuators are designed to ensure its *martensite* form is maintained at room temperature ($20°C \leq M_f$) and recover the 'memorized state' during their *austenite phase* above $50°C$ ($A_s \geq 50°C$).

Electro-mechanical Implemenation

NiTi alloys are especially interesting for actuator implementations as the material itself can form an electro-mechanical actuator. While one could use the hot air stream of, e.g. a hair dryer in order to heat up an SMA, the same effect can be achieved due to *Joule heating*, i.e. by feeding the material with electrical current. Here, the SMA acts as a resistor which heats up under load. Due to the thermo-mechanical behavior of the alloy, this results in a mechanical movement during the *austenite phase*. The resulting mechanical movements and physical forces heavily depend on the programmed shape as well as the form factor of the individually manufactured SMA actuator (see subsection 3.2.3).

NiTi SMAs can be heated up quickly by feeding them with electrical current.

3.2.2 Actuator Characteristics

Some of the most advantageous properties of SMA actuators are the high *force-to-weight ratio*, simple implementation and easy actuation method [Mohd Jani et al. 2014; Qamar et al. 2018]. Their *small size*, *flexibility* and silent operation make them a compelling alternative to traditional electro-mechanical actuators. They can be obtained at low cost in different scales, by means of thickness and length, and allow for a smooth operation. Compared to other smart materials, the manufacturers guarantee high numbers of actuation cycles (up to 10^6) [TOKI Corporation

SMA actuators are simple to implement, have a *small size*, are *flexible* and provide a high *force-to-weight ratio*.

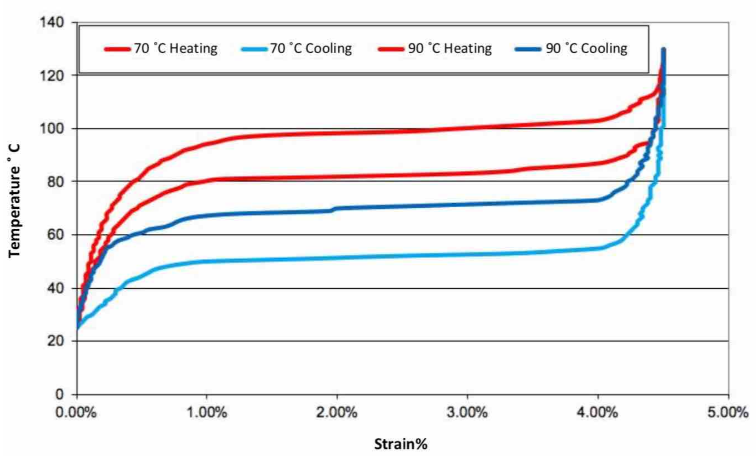

Figure 3.2: Typical Temperature vs. Strain Characteristics of Flexinol® Actuator Wires [DYNALLOY Inc. 2019]. The diagram exemplary shows the nonlinear heating and cooling behavior of SMA wires, as well as the exhibited hysteresis effect.

2017]. While SMA actuators are commonly said to suffer from a low recovery strain, SMA spring actuators significantly increase the recovery strain by a factor of ten (subsection 3.2.3). A known disadvantage depicts the comparable low energy efficiency. Recent work therefore focuses on techniques which allow to improve the energy efficiency. Motzki [2018] suggest that the energy efficiency may be increased by up to 80% using 'high voltage pulses'.

The actuation, however, includes non-linear behavior which is mainly introduced through the heat transfer and a hysteresis effect.

Similar to other shape changing materials such as polymers, the operational characteristics of SMAs include a non-linear actuation behavior which is exemplary shown in Figure 3.2. The difference between the heating and cooling curves furthermore reveal the hysteresis effect which is exhibited by the material. When the thermal stimulus is removed, the material first needs to cool down in order to reach the lower *martensite start temperature* $M_s < A_f$ and allow to recover a certain strain value. SMA actuators can be actuated quickly due to *Jule heating*, but require a larger amount of time to cool down. This consequently forms a bottleneck with respect to the *contraction frequency*. While active cooling is an effective way to perform a higher number of actuation cycles within a fixed period of time, we discuss how different spring actuator implementation techniques can affect the *contraction frequency* in general (see section 3.3.4).

The previously described characteristics are summarized in Table 3.1 and should be considered when building an SMA driven system. Our decision of using SMA actuators for an on-skin application especially bases on their *small size*, *flexibility* and high *force-to-weight ratio*. Compared with traditional actuators, they offer to design unobtrusive interfaces which are thin and allow to align to skin curvatures. They moreover afford to produce smooth motions which do not cause unwanted vibrations and thereby distort our sensory system.

Compared with traditional actuators, the characteristics show to be promising for designing unobtrusive wearable interfaces.

3.2.3 Form Factors

SMA wires and SMA springs belong to the most commonly produced types of NiTi alloy actuators which contract upon actuation. SMA springs are made of SMA wires arranged in coils. Compared to simple SMA wires they provide a relatively high *displacement length*. While SMA wires only contract by roughly 5% of their elongated length, SMA springs can contract by about 50% of their elongated length. This comes along with a decrease of the sustainable stress and a lower generated pulling force during contraction. While a wire with a diameter of $0.2mm$ for example, can pull $570g$, the spring is rated to be able to only pull about $40g$ [DYNALLOY Inc. 2019]. The decision of purchasing an SMA wire or SMA spring actuator therefore always includes a trade-off between the *displacement length* and the pulling force during contraction.

SMA wires provide a high contraction force. SMA springs provide a large *displacement length*.

For our application of a soft skin-drag display, the generated pulling force of most SMA springs is sufficient and we are in particular interested in the *displacement length* of the soft actuators to drag a tactor across a preferably large area on the skin surface.

We are interested in the *displacement length* of SMA springs for our skin-drag display.

advantages	disadvantages
high force-to-weight ratio	heat
flexible	non-linear behavior
scalable form factors	hysteresis
cheap	low-moderate frequency
silent & smooth operation	(low energy efficiency)

Table 3.1: Thermal One-way SMA Actuator Characteristics

3.3 Basic Spring Actuator Implementation

FLEXINOL 90°C Spring

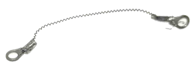

BMX150 Helical Spring

For our experimental tests we used BioMetal Helix actuators and FLEXINOL® 90° Actuator Springs [TOKI Corporation 2017; DYNALLOY Inc. 2019]. The provided information in the datasheets may vary between the different manufacturers. In the following we will describe which parameters are most meaningful for the design and operation of spring actuators, as well as how one may derive parameters that are not explicitly mentioned in the datasheets.

3.3.1 Physical Design Parameters

When implementing SMA springs, the most important parameters comprise their minimal *contracted length* and their maximal *elongated length*.

SMA spring actuators usually can be purchased at different scales based on their *solid length* L_S or the number of coils $\#coils$. The *solid length* depicts the spring length at which the actuators are manufactured and shipped. The *solid length* can be derived by multiplying the *wire diameter* D_W with the number of coils: $L_S = \#coils \times D_W$. However, as illustrated in Figure 3.3 the *solid length* usually cannot be fully recovered during operation. The manufacturer therefore only provides approximate information about the actuators characteristics based on a 'hot length' which we will refer to as the actual *contracted length* L_C and the 'cooled' *elongated length* L_E. To estimate the contracted and *elongated length* the manufacturer may provide certain *stretch ratio* values (SR_C and SR_E) relative to the solid length. In this case the individual parameters usually can be calculated by $L_C = L_S \times SR_C$ and $L_E = L_S \times SR_E$. Consequently the *displacement length* is given by $L_D = L_E - L_C$. Alternatively, the manufacturer may also provide a *displace-*

ment factor d_F which allows to obtain the *displacement length* based on the number of coils $L_D = d_F \times \#coils$ (or based on the contracted length $L_D = d_F \times L_C$). As stated earlier these values usually still remain rough estimates as the SMAs' behavior can be influenced by several environmental factors and varying load during operation. Hence, it is

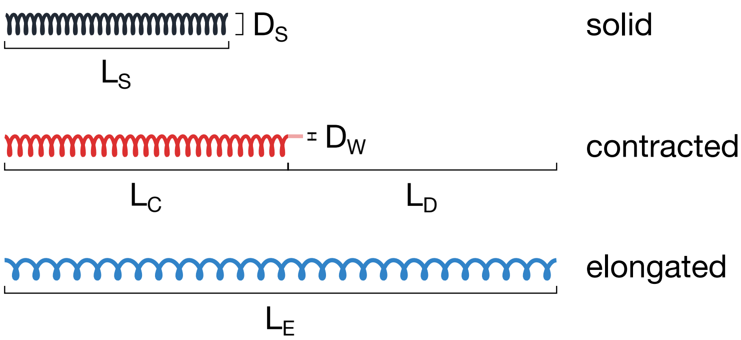

Figure 3.3: SMA Spring Design Parameters

recommended to examine and verify these values experimentally for an individual application by performing repeated contractions. It should further be noted that the implementation requires crimping the springs to terminals as soldering thermal SMAs usually causes permanent damage to the soft actuators. The number of the remaining, effectively used coils after the assembly are commonly referred to as the number of *active coils* ($\#activecoils$) which should be considered when purchasing the springs or verifying operational characteristics.

3.3.2 Control Parameters

As discussed in subsection 3.2.3, SMA actuators are commonly designed to provide a high *contraction force* or a large *displacement length*. These variables are of greatest interest for most applications along with the *contraction frequency*. While shape and dimension of an SMA actuator define the general operational boundaries and magnitude of these variables, further parameters such as *time*, *current*, *temperature* and *stress thresholds* are meaningful for the control of a spring actuator.

Usually a recommended *current value* is provided along with an estimated *contraction time* for a proper operation to reach the specified *contraction force*. Based on the recommended *cooling time* one may derive the *contraction frequency*. The provided values however still should be treated as rough estimates. If a resistance by length factor R_F is only provided based on the straight SMA wire, one can derive an estimate for the corresponding spring resistance by $R_{SMA} = R_F \times \pi \times D_S \times \#activecoils$.

As long as as the upper *stress and temperature limits* are not exceeded, other control values may vary from the recommended ones.

The power values such as the drawn current are typically not limited to the specified ones and can exceed the recommended values without harming the actuator. The most critical factors which should be considered are sustainable stress limits and an upper temperature threshold in order to prevent an actuator from overheating. The manufacturer only guarantees a long operation lifetime and high number of repeated contractions below these thresholds. While the critical stress limits are usually given and correlate with the recommended *contraction force*, the upper temperature threshold which may comprise the *austenite finish temperature* A_f is not necessary given. For Flexinol Spring Actuatores, e.g. only a rough estimate for the *transformation threshold* is provided, namely $70°C$ or $90°C$. Hence, one may experimentally derive a threshold by investigating on the temperature at which the *contraction length* L_C is reached under the recommended load. The question may arise, why one would want to exceed the recommended values. The higher the current flow, the faster the SMA heats up. This may be desired in order to achieve a quicker response regarding the contraction time when the SMA has to heat up from a low temperature. As Figure 3.2 indicates, there is also a non-linear relationship between temperature and strain one may want to overcome. In any case, higher current loads should only be applied for a short fraction of time as the SMA can quickly heat up and exceed the recommended temperature threshold.

Altering the power over time apparently depicts the most effective way of manipulating the contraction force which is discussed in the following.

3.3.3 Basic Control of a Contraction

A basic contraction can be triggered by crimping electric cables to the SMAs' tails and attaching them to a power supply such as a simple battery (see Figure 3.4a). A switch may be used to start and stop feeding the SMA spring with current. As the SMA acts as simple conductor with a resistive heating effect, it can be treated as a simple resistor. The amount of current which is drawn may therefore be directly derived by Ohm's law. However, the resistance depends on the form factor and may slightly vary during actuation about 1Ω (see section 3.3.5). This binary control method usually causes a 'snapping effect' when the SMA heats up quickly and reaches the *tranformation threshold*. While this behavior may be sufficient or even desired for certain applications, a more advanced control may be of interest which allows to control the contraction time and prevent the actuator from overheating.

In order to control the contraction time and power of an SMA spring in a continuous way, one has to get in control of the drawn current. This can be achieved by using a logic controller which generates a PWM signal and a transistor as illustrated in Figure 3.4b. As the output pins of a microcontroller typically only provide a limited current per pin (e.g. $40mA$ for I/O pins of an ATmega328), a transistor is integrated to allow to feed the spring with higher currents ($250mA$ up to multiple amperes). In a real application it

SMAs need to be powered carefully as they can overheat quickly – resulting in permanent damage.

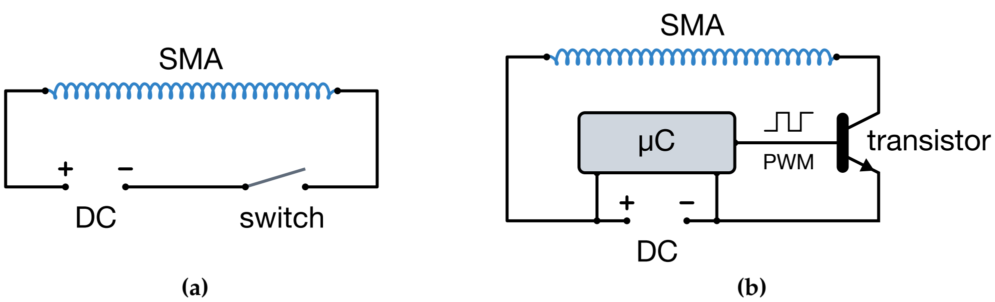

Figure 3.4: Simple schematic of a most basic (binary) SMA spring contraction control (a); a logic controller is used in order to control the contraction time and modulate the power (b).

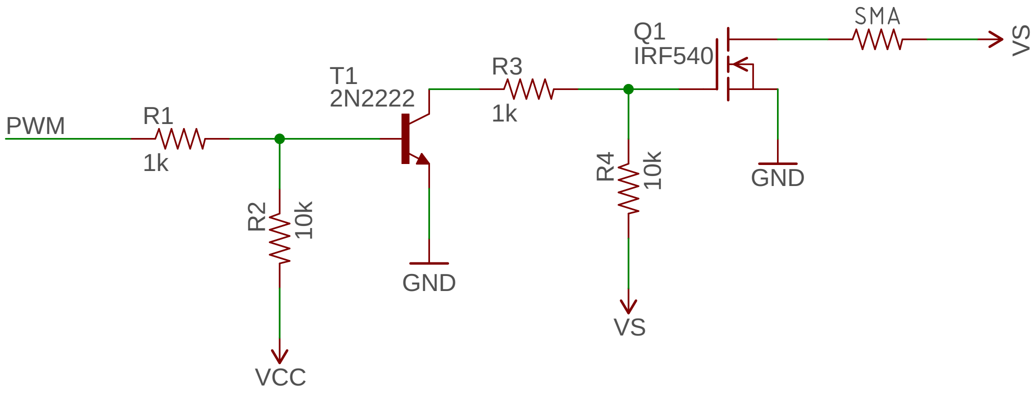

Figure 3.5: A gate driver allows to control very high loads through a PWM signal of a microcontroller. Here, V_{CC} describes the logic power level and V_S the higher source power voltage. As the power of the microcontroller is too weak to control the IRF540 MOSFET, an additional 2N2222 transistor is required to amplify the logic output signal.

may furthermore be desired to drive the SMA at a higher voltage level than the logic power supply. In this case a gate driver is commonly implemented instead of a sole transistor. Figure 3.5 shows a schematic which uses an IRF540 MOSFET as power amplifier and embeds a 2N2222 transistor as 'level shifter'. By using a PWM signal of the microcontroller one can this way gain linear control about the electrical current flow depending on the duty-cycle. The IRF540 supports very high current loads which is sufficient to drive bigger scaled SMA spring actuators such as Flexinol Actuators with a spring diameter of $D_S = 3.45mm$.

3.3.4 Repeated Contractions

The SMA spring only contracts upon actuation; a *bias force* is required in order to elongate it and allow for multiple contractions.

So far we only described how to roughly control and trigger a single contraction of an SMA spring. But since NiTi SMA springs have a *one-way SME*, the spring will not elongate on its own afterwards and allow for a repeated contraction. Hence, a *bias force* is required which pulls back the spring. This can be achieved by using a normal mechanical spring which provides a *passive bias force* in the opposite direction (Figure 3.6). We will call the joint which connects the SMA spring and the mechanical spring the *operation*

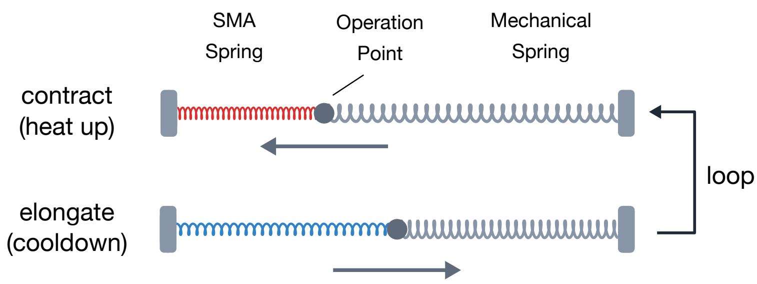

Figure 3.6: SMA spring (left) and mechanical bias spring (right) pull the *operation point* from one side to the other.

point. The *operation point* is usually of interest when pulling an object such as a tactor. As the mechanical spring has to be weak enough to let the SMA spring easily contract and strong enough to pull the *operation point* completely back, some manufacturers provide a mechanical spring tailored to these demands. Depending on the application the bias force may also be provided by some elastic matter such as our skin. Instead of a passive bias force, moreover, another SMA spring may be used in order to provide an *active bias force* which can be beneficial to gain even more control of the *operation point's* position.

Whether an *active* or *passive bias force* is appropriate to use depends on the application. On one side, a mechanical spring can offer a quite reliable *passive bias force*. The material properties may be well known and less prone to environmental factors such as the temperature. It furthermore does not have to be integrated into a circuit; and if the bias force is provided by the pulled object itself, such as the skin, it can even save space. On the other side, the SMA spring has to overcome an additional force and looses efficiency if the control of an *operation point* is of interest. The SMA needs to be constantly actuated in order to retain the current position of the *operation point*. In contrast, an *active bias force* which is provided by an antagonistic SMA spring, may only provide a bias force if wanted. It therefore allows to maintain the position of the *operation point* after the actuation more easily. A second SMA spring furthermore allows to variate the bias force. As less work is required in order to move the *operation point* (i.e. the tactor) and the

An *active bias force* provides more control about the *operation point*, but introduces complexity and may require more space.

contraction point can be pulled even stronger after actuation, one may even increase the *contraction frequency* this way.

Contraction Frequency

As the spring actuator needs to cool down in order to transform back to the *martensite* phase and completely elongate again, a common drawback of SMA spring actuators is said to be the low-to-moderate *contraction frequency*. Without the help of any additional cooling system one can usually assume a safe *contraction frequency* of $0.1Hz$ at room temperature. Nevertheless, depending on the environmental factor higher or lower frequencies may be obtained.

Active vs. Passive Configuration Test

As discussed before, it is liable that replacing a mechanical *passive bias spring* by an *active antagonistic SMA spring* would provide more control and even increase the *contraction frequency*. We aimed to verify the latter by comparing the *contraction frequency* of a BMX150 Helical Spring within an active antagonistic configuration and a passive configuration similar to Figure 3.6.

We compared a passive mechanical spring to an active SMA spring which functioned as bias force.

SETUP & PROCEDURE: The test was performed using a mechanical bias spring provided by the manufacturer together with the BMX150 first, and then replacing the passive bias spring with another BMX150 Helical Spring. The latter, i.e. the *active configuration* is shown in Figure 3.7. The test was performed in a controlled environment at $21.9°C$ with a steady power supply ($7.98V$), the drawn current was limited and measured to be $251mA$. We set the contraction time of the SMA actuators to constant $2sec$ and the relax time (initial cooldown time) to $10sec$. A complete cycle for the *passive configuration* consisted of a contraction followed by a relax phase. A complete cycle for the *active configuration* consisted of a cooldown phase followed by a contraction of the first SMA and another cooldown and contrac-

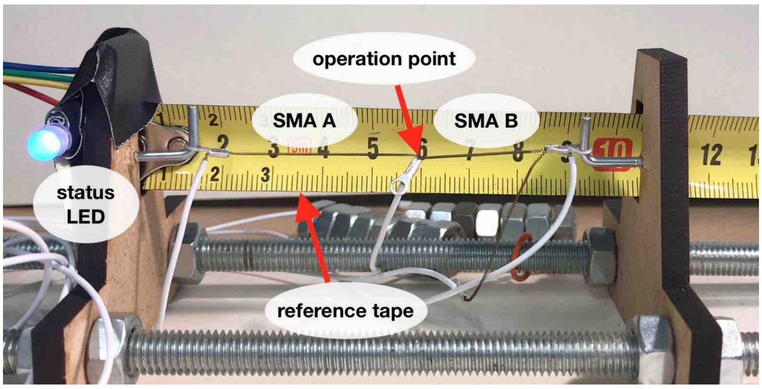

Figure 3.7: Two SMAs actively pulling the *operation point* back and forth. An LED indicates which SMA is currently pulling. A measuring tape serves as reference for tracking the displacement of the *operation point*.

tion phase of the second SMA. Each complete cycle was performed 10 times.

The *active configuration* increased the *contraction frequency* from $0.1Hz$ to $0.167Hz$.

RESULTS: The *passive bias spring* required $8sec$ to fully elongate the SMA spring after $2sec$ actuation. Hence, $2 + 8 = 10sec$ were required for a complete cycle of the *passive configuration* ($7.5mm$ displacement). For the *active configuration*, the cooldown time was steadily decreased from $10sec$ to $0sec$. The *active configuration* showed to be able to retain the same *displacement length* with a cooldown time of $1sec$. Consequently only $(2 + 1) + (2 + 1) = 6sec$ were required for a complete cycle which is a difference of $4sec$. Hence, the *active bias force* indeed increased the *contraction frequency* from $0.1Hz$ to $0.167Hz$. It should be noted that we assume that only the actuation in one way is of interest in this case. Apparently, an *active configuration* of two antagonistic actuators is even more advantageous if both contractions are meaningful to the system. While the mechanical spring would in this case still limit the *contraction frequency* to $0.125Hz$ in one direction, the *contraction frequency* of the *active configuration* doubles to $0.33Hz$ and allows for more homogeneous and controlled actuation cycles.

3.3.5 Closed Loop Control

A feedback system which provides information about the system state could provide more accurate control about the actuators.

The non-linear behavior of the actuators is commonly known to complicate modeling and predicting the actuators behavior accurately regarding the various effects such as the occurring heat transfer and hysteresis. A generalized model especially appears difficult as these effects may strongly depend on the form factor along with the alloys' composition or the way of how the actuators are integrated into a system. A typical workaround is to implement a closed feedback-loop in order to compare a reference value to the actual system state and readjust the control parameters for minimizing the measured error. While this may be achieved using an external sensing system these tend to dramatically increase the size of the apparatus.

Self Sensing Test

Several work suggests that one can monitor the displacement by measuring the resistance of an SMA wire.

Several work suggests that the metal alloys allow to establish a feedback loop by measuring the SMAs' resistance itself as there appears to be an almost linear strain-to-resistance relationship [Lewis et al. 2013; Josephine Selvarani Ruth et al. 2014; Cho et al. 2010; Ma et al. 2004]. As this control method would be most preferable in order to keep a potential on-skin actuation system as small as possible we aimed to test the feasibility of a self sensing system similar to Wang et al. [2012].

We investigated on the displacement vs. resistance relation of SMA springs using a simple setup.

SETUP & PROCEDURE: For this test we used a $90°C$ Flexinol Actuator Spring ($D_S = 1.37mm$). An Arduino UNO connected to a steady power supply ($V_{in} = 4.75V$) was used in order to derive approximate values for the resistance. We implemented a simple voltage divider comprising a high current power resistor ($R_0 = 5.5\Omega$); the voltage drop V_{out} was measured using an analog input pin of the Arduino UNO. As $R_0 < R_{SMA}$ the resistance was then calculated by:

$$R_{SMA} = \frac{R_0}{(\frac{V_{in}}{V_{out}} - 1)} \tag{3.1}$$

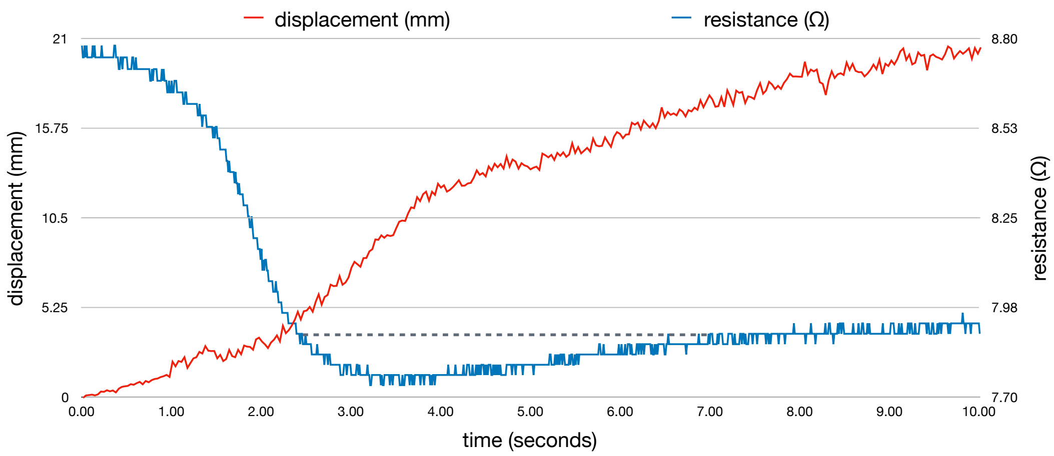

Figure 3.8: SMA Spring Resistance vs. Displacement: Due to the non-linear and non-monotonic behavior, it reveals to be hard to derive a direct estimate for the displacement from the measured resistance.

The actuation was recorded on video and the relative *displacement length* derived by tracking the *operation point* using a video analysis tool.

RESULTS: Although the measured values shown in Figure 3.8 only depict rough estimates, the results showed that we can indeed observe a correlation between the measured resistance and recovery strain which is, however, certainly not of linear nature (critical range indicated by a dashed line). Especially above a threshold of approximately 50% of the effective *displacement length* the measured values showed critical fluctuations, making an accurate control based on a simple self sensing system infeasible. A setup using a differential amplifier and controlling the power through PWM introduced even more complexity for measuring the resistance due to the non-analog output signal. While we could facilitate a preliminary workaround by implementing a constant measurement interval, we obtained similar results. The measured signal unveiled to be very unstable above 50% of the contraction.

The measurements let suggest that the resistance does not provide a reliable reference value to establish a robust feedback system for spring actuators.

Due to the observed instability of our self sensing system, we decided move on with a provisional open-loop system, as we aimed to keep the system size as small as possible. At this point it should be noted that we do not want to pre-

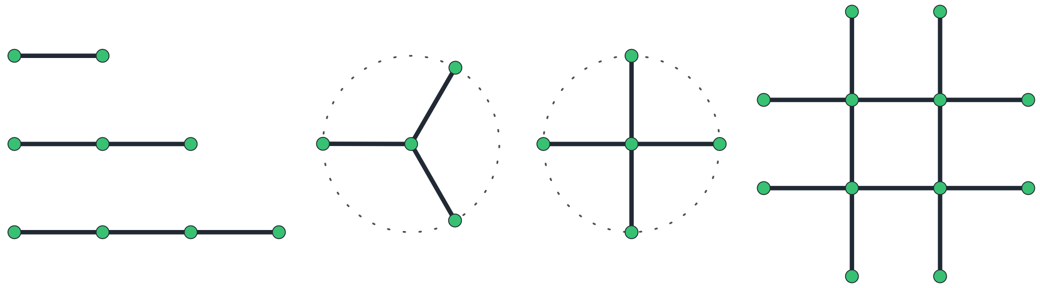

Figure 3.9: Different Topologies (left to right): simple chaining of SMA actuators; 3-star topology; 4-star topology; 2x2 mesh (with outer extension). Nodes indicated in green; connections as black lines.

clude a potentially robust self sensing control system for SMA spring actuators; our assumptions may be based on a poor measuring method and limited expertise. However, we noticed that existing literature appears to exclusively focus on SMA wires. The lack of existing work providing evidence regarding the feasibility of such a system for SMA spring actuators, therefore may indicate an interesting point for future work.

3.4 Advanced Spring Actuator Control and Implementation Concepts

We have already introduced an *antagonistic configuration* within which we used two instead of one actuator. In this section we will mainly discuss how one may implement multiple actuators and realize a control for more advanced topologies in order to produce different on-skin sensations.

3.4.1 Topologies

While on-skin applications may take advantage of completely different implementations and configurations of spring actuators, we propose three different types of topologies which are easy to realize and could be of interest for on-skin applications. Figure 3.9 exemplary shows:

- one-dimensional chaining of n actuators
- two different star topologies (n-star topology)
- a mesh of SMA actuators ($n \times n$-mesh)

In the following, a *connection* is always defined by two *nodes*. We further assume that in each case every *connection* depicts an SMA actuator (or fraction, see subsection 3.4.2) of equal length which are supposed to be controlled. *Nodes* may be attached to stiff as well as elastic matter such as a frame or the skin. Alternatively, one can imagine to use a node in order to move an object like a tactor across the skin. Independent of the attachment of a *node*, we assume every *node* is required to be wired and integrated into a circuit in order to control any of the *connections*. In the following, our interest especially relies on the attachment and integration of the *nodes*.

We show how one can easily implement and control different topolgies using SMA actuators.

3.4.2 Connecting Multiple SMA Actuators

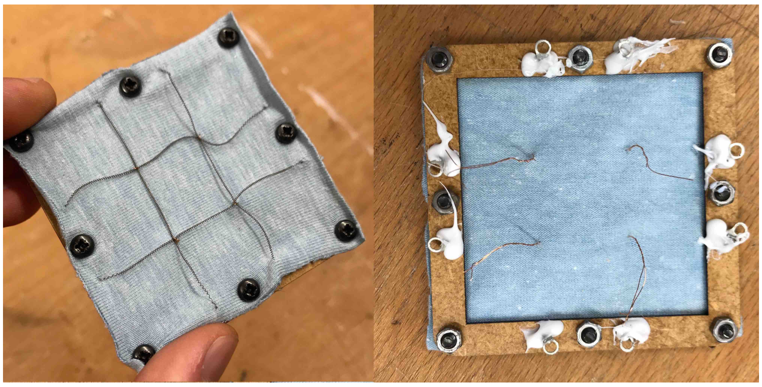

Figure 3.10: Top and bottom view of a prototype for a 2×2-mesh using four BioMetal Helix actuators attached to a solid frame. The actuators are connected at the intersection points by twisting and crimping simple copper wires which allow to access the individual nodes. We used a flexible textile to simulate and test the elastic behavior of the skin.

An interesting property of SMA actuators is that they commonly consist of the raw metal alloy and provide uniform

The smart material allows to easily interconnect multiple actuators by interweaving and crimping them together.

conductivity across the whole surface. Therefore, one may connect two separate actuators through a joint or just use a single spring of doubled length and attach an electric wire in between to gain control of the different parts. This is especially interesting for the proposed $n \times n$-mesh topology which can be less tedious to fabricate at larger scale as no complex joints are required for coupling four SMA ends plus a wire connector at the individual node. We will refer to a *node* which is shared by multiple *connections* as their *common node*.

Obviously, we define our mesh by the number of SMA actuators which are interconnected in the previously described manner. With this definition of a $n \times n$-mesh, the illustrated 4-star topology may therefore also depict a special case and be treated as a 1×1-mesh. Figure 3.10 shows a prototype for the proposed 2×2-mesh topology which demonstrates the simple way of interconnecting several actuators for more advanced control configurations.

This way, rigid parts and complexity can be moved from the on-skin interface to the control unit.

To illustrate how valuable this method of connecting multiple SMAs is, we can estimate the number of connections required for a generalized $n \times n$-mesh $\#conn = 2n(n+1)$. Likewise the number of nodes is given by $\#nodes = 4n + n^2$. Hence, we save $2 \times \#conn - \#nodes = 3n^2$ wires for a $n \times n$-mesh. Apart from simplifying the fabrication and electric wiring, one may this way retain a more flexible structure, as the joints usually introduce stiff parts such as rigid terminals.

3.4.3 Controlling Multiple Nodes

So far, we only showed how to realize the control for a single actuator or a chain of two actuators. However, our prior control concept (from subsection 3.3.3) may not apply for all topologies. By connecting multiple SMAs directly, the resulting chain or mesh forms a single conductor. Hence, one has to consider the current flow more carefully in order to actuate the desired connections properly.

In many cases, alternating the polarity can be sufficient. Regarding our antagonistic setup incorporating two SMA actuators, e.g. we could connect the voltage source VS directly to the *common node* at the center and choose to control the current flow through an N-channel MOSFET for the individual connection at the outer nodes. This concept would also apply for star topologies. For longer chains of actuators and a $n \times n$-mesh this concept does not apply. As the current flow would not be limited in one direction, only controlling nodes regarding a certain polarity may cause the actuation of multiple connections. One solution could be to alternate the polarity and control each node using a single MOSFET. A more powerful control circuit which would apply for any kind of topology could take advantage of a set of half-bridges and allow for controlling the polarity of the individual nodes. The latter would come with two advantages: (1) we retain a reduced number of nodes. (2) a half-bridge allows to define three states VCC, GND, OFF HIGH-Z for each node. One could this way obtain a programmable mesh of SMA actuators which does not only allow to control any connection between two neighboring nodes, but also the current flow through larger parts of the mesh, including multiple path-ways and connections. We show how we realized a controller board implementing a programmable set of half-bridges in subsection 3.4.5.

In most cases it is sufficient to control the current flow as well as the polarity of the individual nodes using a simple MOSFET.

Half-bridge Output Control

In Figure 3.11, we show a schematic which allows to control the state and polarity of one output PIN in a continuous way. The schematic still allows to control large currents and extends our previous control concept (see Figure 3.5) in a simple way. The major difference relies in the implementation of the second MOSFET $Q2$. Nevertheless, in this case the logic controller has to deliberately control IN01 and IN02 for changing the output of OUT01. OUT01 is considered to be connected to a node. Table 3.2 shows the effect of different input levels and the resulting output mode for a binary voltage control (LOW, HIGH). Note that the logic is inverted because of our chosen MOSFETs. Hence, a logic 1 equals to LOW voltage. The circuit furthermore allows for a dangerous state. If the inputs are set to LOW, both

By using a half-bridge for each node, more advanced topologies can be programmed and controlled dynamically.

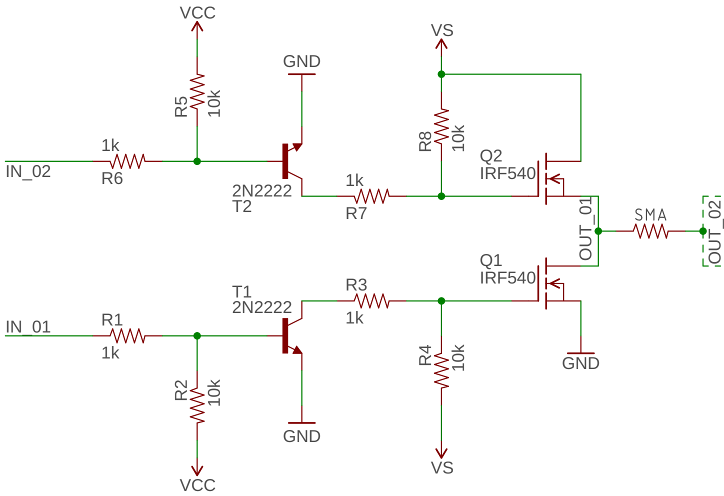

Figure 3.11: Schematic of a simple half-bridge output which allows to control the polarity of a node. A logic controller can manipulate the output pin by controlling two inputs.

MOSFETs are turned on causing a short which should be prevented in any case. While the table only shows a binary control of the output state, one may still facilitate a linear control of the current flow by keeping one input at the HIGH voltage level and controlling the PWM signal of the other.

IN01	IN02	OUT
LOW	HIGH	GND
HIGH	LOW	VCC
HIGH	HIGH	OFF (HIGH-Z)
LOW	LOW	short (critical)

Table 3.2: Half-bridge Output Logic
Next to the three desired states, the circuit allows for a critical state. A short circuit should be prevented in any case by ensuring at least one input to be set HIGH.

3.4.4 Body Grounding

Even though general body grounding concepts (i.e. how different topologies may be attached deliberately to the skin) are beyond the scope of this thesis, we will briefly discuss some general ideas. For on-skin applications using SMA spring actuators our primary interest relies on using the lateral contraction of a spring in order to produce any kind of sensation. However, the spring as a raw, generates a uniform *contraction force* on both sides. Depending on the application, one may want to produce a directional pull which requires at least grounding either of the sides to the skin. For body-grounded devices this may be achieved by carefully distributing the force due to a certain shape or type of the body grounding material (i.e. the attachment layer). Hamdan et al. [2019] for example, designed a sticker which uses a SMA spring mounted on a triangle shaped attachment layer, such that the stimuli on one side produces a relatively weak sensation compared to the other and causes a directional skin-stretch.

Within our initial tests, the SMAs could be grounded to a solid frame fixed on a table. For on-skin applications one has to carefully consider how to attach the interface to the skin in order to produce the desired sensations.

In an ideal case a deliberately designed system considers that the produced stimuli is below the activation threshold of certain mechanoreceptors. Important factors may depict the *spatial dimension*, *viscosity* and *friction* of the grounding material, the *force magnitude*, as well as the *number of activated receptors* which may depend on their *activation threshold* and *receptive field*.

3.4.5 Generic Controller Board

We designed a generic controller board (Figure 3.12) which allows to control any of the previously mentioned topologies or several distinct SMA actuators. The board allows to control 12 half-bridge output pins, i.e. nodes, by using a TLE94112 driver module and only measures an outer dimension of $40mm \times 25mm \times 7mm$. A $9V$ battery can be connected to a power socket and a bluetooth module allows to control the actuators via wireless communication. A detailed schematic can be found in Appendix A.

We developed a generic controller board which allows to program and control 12 independent nodes as proposed previously.

We tested the control of our 2×2-mesh prototype with our controller board which showed to be capable of providing basic control of each output pin as desired for our setup. While we could already control the individual actuation of different connections, we faced several limitations due to the implemented driver module. First of all, the current was limited to about $0.9A$ and the integrated protection could quickly shutdown the driver module when actuating multiple SMAs. Secondly, the driver module only allowed to assign a PWM signal to 3 of the 12 pins at once. Hence, only the current flow of three connections could be controlled continuously at a time. Because of the communication protocol, a software PWM turned out to be infeasible as the communication overhead introduced a bottleneck for multiplexing, in general. Finally, for longer operation the driver heated up, causing a driver shutdown through the integrated heat protection.

While we could show that the control unit can be miniaturized, we faced some bottlenecks. It was decided to postpone fixing these as part of future work.

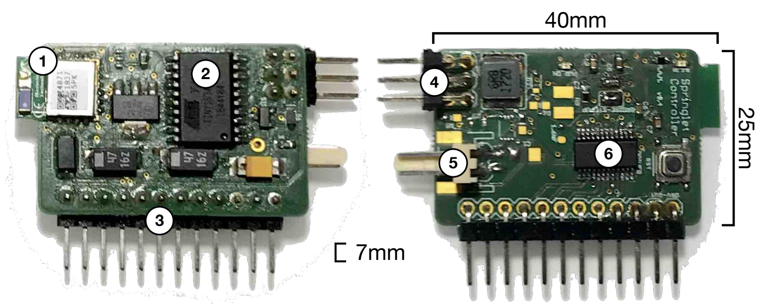

Figure 3.12: Small sized $(40 \times 25 \times 7mm)$ controller board for 12 nodes (top+bottom): RN-4871 Bluetooth module (1); ATTINY1634 logic controller (2); 12 half-bridge outputs (3); programming interface (SPI) (4); battery power socket (5); TLE94112 driver (6).

Nevertheless, we assume that exchanging the implemented driver module with an appropriate one could resolve these issues and allow for a wireless control of different and more complex actuator configurations as discussed before. Beyond the driver module, our controller board already reveals promising characteristics for a preferably unobtrusive wearable interface due to its small size and compact form factor.

Chapter 4

Skin-drag Display

Based on the implementation concepts and gathered experiences as described in chapter 3, we aimed to develop a first prototype of a wearable and soft skin-drag display which allows to plot diverse two-dimensional skin-drag gestures on the skin.

In order to achieve this, we first designed a display using several SMA spring actuators to generate skin-drag sensations by dragging a tactor, i.e. a small object, across the skin surface. Secondly, we developed a control system which manipulates the SMA actuators according to our control model, such that our device could perform timely controlled movements.

4.1 Display Design

To move a tactor in two dimensions, we decided to use a star topology of four antagonistic SMA spring actuators as illustrated in Figure 4.1a. The SMAs were connected at a *common node* and attached to the fixed *anchor points* A_0, A_1, A_2, A_3. The contraction of the individual SMA springs would therefore allow to manipulate the position of the tactor by pulling it towards the corresponding *anchor point*.

The display uses four SMAs in order to pull and move the tactor in two dimensions.

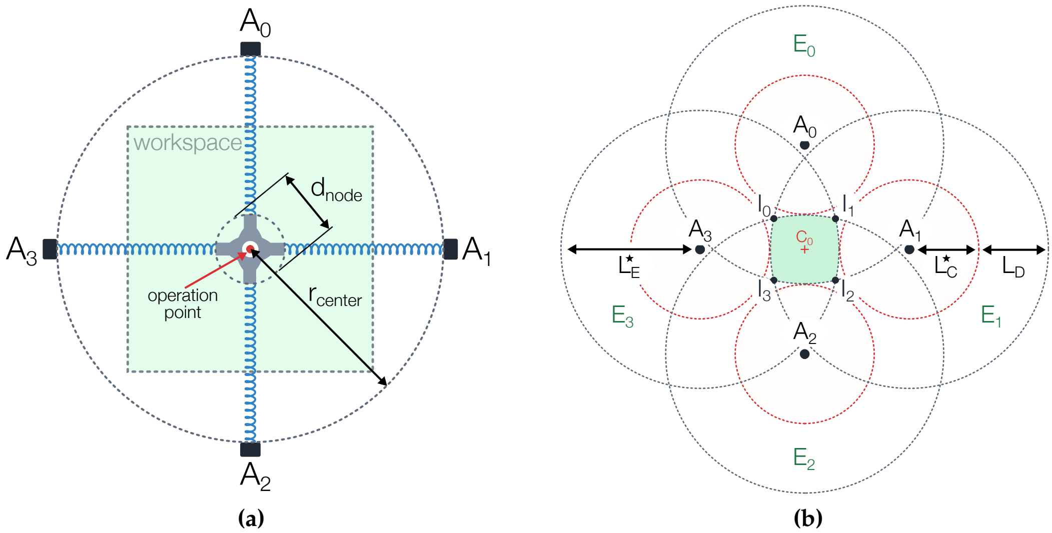

Figure 4.1: Design parameters of the 4-star topology using SMA springs: (a) shows the four SMA springs (blue) connected to the *anchor points* A_i and a *common node* forming the *operation point* at the center; (b) shows the most important design parameters to derive the *effective movement area* (green) which is restricted by the annuli E_i.

Design Decision Justification:
3-Star vs. 4-Star Topology

3-STAR VS. 4-STAR TOPOLOGY:
We chose a configuration with four antagonistic operating SMAs over three, as we could this way obtain a larger *effective movement area* (*EMA*) for our target application. Compared to a 3-star topology as proposed by [Kolyvas and Tzes 2018], the resulting EMA is furthermore *convex* and provides a *higher degree of axial symmetry* (Figure 4.2). We assumed that we could this way (1) support a higher number of distinguishable gestures on the skin, and (2) obtain more accurate control of the tactor being attached to the *common node*.

The *anchor points* A_i $(1 \leq i \leq 4)$ of the SMA springs were evenly distributed around the center point C_0. By considering the diameter of the *common node*, the distance between the SMA *anchor points* and the center point is given by $r_{center} = \frac{L_E+L_C+d_{node}}{2}$.

With the proposed configuration the tactor could move within an effective movement area (EMA) which is limited

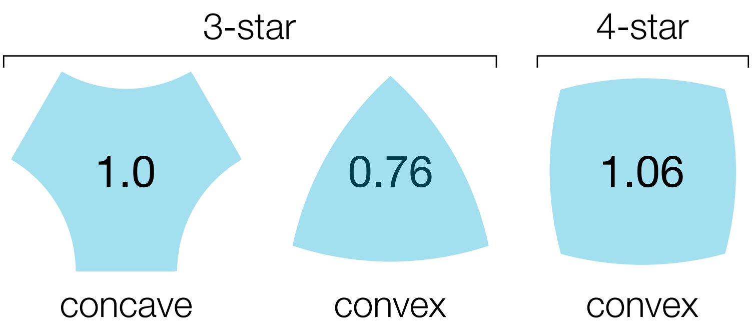

Figure 4.2: Maximized EMA for a 3-star topology proposed by Kolyvas and Tzes [2018] (concave, left); our 4-star topology shows to benefit from a convex shape and yield in a ($\sim 6\%$) larger EMA (right).

by the minimal *contracted length* L_C and the maximal *elongated length* L_E of the SMAs. Hence, the exact EMA is given by the intersection of the annuli E_i being bound to the concentric circles at the *anchor points* A_i, with the inner radius $L_C^* = L_C + \frac{d_{node}}{2}$ and the outer radius $L_E^* = L_E + \frac{d_{node}}{2}$ (Figure 4.1b). We moreover chose the intersection points I_i of the outer circles with the center points A_i and a radius of L_E^* to span our *workspace*. By doing so we obtained a rectangular *workspace* area with its origin at I_3. This allowed us to define a point in a *Cartesian coordinate system* for our two-dimensional motion system.

The effective movement area is restricted by the contracted and the elongated spring lengths.

4.2 Control Model

While our display design ensured to meet the mechanical requirements for a positional control of the *tactor*, the spring actuators had to be controlled in a deliberate way. This could be achieved by supplying the SMAs with the right amount of current for a given amount of time, such that the *tactor* would perform the intended movements and produce the desired skin-drag gestures.

The control model defines how much current is supplied to the individual SMAs for a given amount of time.

We developed a *hybrid model* which allowed us to control our proposed configuration of four antagonistic SMAs without the need of an additional sensory system. The *hy-*

brid model builds on two basic models we investigated on in advance. The assumptions made, as well as the individual advantages and disadvantages which lead to our final model are being discussed in the following.

Design Decision Justification: *Open-loop Control*

Open-loop Control:
Although a closed-loop control would have been most preferable for accurately controlling the skin-drag display, we chose to rely on an *open-loop control system* because of the following three reasons:

(1) Despite previous work indicates that the self-sensing capability of SMA actuators could be used in order to realize a closed-loop control system [Josephine Selvarani Ruth et al. 2014; Lewis et al. 2013; Wang et al. 2012; Cho et al. 2010; Ma et al. 2004], the proposed systems unveiled to exclusively focus on SMA wire actuators. Our initial tests with SMA springs, however, revealed difficulties regarding the precise control of an *operation point* based on the strain-resistance correlation (section 3.3.5). Since Furst et al. [2013] let suggest that a more complex topology would make a self-sensing system even less reliable due to the reciprocal influence of multiple interconnected SMAs, we rejected the idea of implementing a feedback-loop by measuring the resistance.

(2) As an alternative way to establish a closed-loop control system, we considered using an external sensing system which could provide feedback about the *operation point's* position. However, we aimed to keep the display in a most simple form with focus on the system size and it's wearability.

(3) Even with positional information about the *operation point*, diverse non-linearities such as the heat transfer and the hysteresis effect would have to be taken into account for an accurate control (subsection 3.2.2).

4.2.1 Force Equilibrium Model

Our first model relied on the assumption that any point within the defined workspace could be mapped to a unique power ratio for the spring actuators, such that the pulling forces of our antagonistic system would cancel out at a desired target position p_j. Regardless of the prior position, the resultant force at the *operation point* p_{op} for $p_{op} \neq p_j$ would consequently pull the *tactor* towards p_j until the force equilibrium is reached, i.e the net force is equal to zero (Figure 4.3).

To acquire an arbitrary target position, a unique force ratio between all four SMAs is calculated.

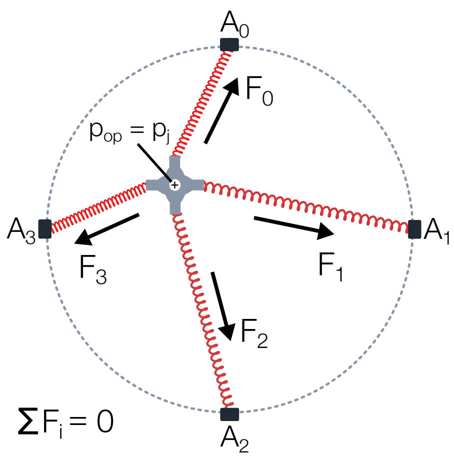

Figure 4.3: The contraction of the individual SMAs (red) provides a pulling force F_i towards the corresponding *anchor point* A_i.

Despite diverse non-linear effects we found, that for a safe maximum power value P_{max}, we could assume a linear power-strain relation to determine the required power ratio for an arbitrary position p_j. The power level of SMA S_i and a target position p_j was calculated by $P_{ij} = \frac{L_E^* - d_i}{L_E^* - L_C^*} \times P_{max}$, where $d_i = \|p_j - A_i\|_2$ describes the distance between the target point p_j and the *anchor point* A_i for the corresponding SMA.

Discussion

Positions can be acquired accurately without a feedback loop. The required time is hard to predict.

The greatest benefit of this model was that an arbitrary position could be reached regardless of the prior position and thus allowed for an open-loop operation. However, the maximum power P_{max} which had to ensure that the pulling force of an SMA would not exceed the stress limit of other antagonistic actuators resulted in slow acquisition times. We found that at least ten seconds were required in order to ensure that the target position is reached from any prior position. In addition, all actuators were required to be actuated at once. Hence, we would not be able to obtain fast movements or increase the actuation frequency similar to our previously performed tests (see section 3.3.4). Finally, without modeling any non-linear behavior of the system, timely controlled movements appeared to be infeasible to realize.

4.2.2 Boosted Movements Model

Our second approach based on the idea of performing relative movements by pulling the *operation point* using maximal two instead of all four SMA springs. As the remaining SMAs would not provide a bias force we assumed that movements could be performed faster and the actuators be driven at higher power levels without harming the inactive actuators.

Relative movements are performed using maximal two SMA actuators.

The realization of this model required three major considerations in order to perform a relative movement:

1. The identification of the required SMA actuators
2. The determination of the individual actuation power
3. The estimation of the required actuation time

Because of our symmetrical actuator design and defined coordinate system, the required (active) SMAs for a movement m_j could be easily identified based on the sign of the axis components of the direction vector $\vec{r} = p_j - p_{j-1}$. The calculation of the individual actuation power for a movement based on the force ratio of two active SMAs revealed to be more difficult due to the strong non-linear behavior of SMA spring actuators (see subsection 3.2.2).

Therefore, we took a most basic approach and first investigated on the *time-distance-power* relation $T_p(d)$ of a single SMA spring by performing multiple contractions at different power levels $\leq P^*_{max}$. Based on the measurements of repeated contractions we initially determined a spline $t(x)$ as a function of distance to estimate the actuation time at 50% of the maximum actuation power P^*_{max}:

The non-linear actuation behavior of a single SMA was modeled in a most basic way by investigating on the *time-distance-power* relation.

$$t(x) = \begin{cases} s_1(x) & 0 \leq x < 0.055 \\ s_2(x) & 0.055 \leq x < 21.11508198 \\ s_3(x) & 21.11508198 \leq x \end{cases} \tag{4.1}$$

The exact polynomials $s_1(x), s_2(x), s_3(x)$ can be found in Appendix C.

As the function approximated the measuring series at other power levels by non-uniform scaling, we inferred a parametrization of $t(x)$ by the power value p with the scaling exponents $g(p)$ and $h(p)$:

$$g(p) = 0.9988849 + \frac{1.288355 - 0.9988849}{1 + (\frac{p}{12.14066})^{4.240305}} \tag{4.2}$$

$$h(p) = 0.8391275 + \frac{1.347852 - 0.8391275}{1 + (\frac{p}{25.38628})^{1.347124}} \tag{4.3}$$

The parametrized function which describes the non-linear *time-distance-power* relation is given by:

$$T_p(d) = t(d^{g(p)})^{h(p)} \tag{4.4}$$

Our poor method of paramaterization resulted in a scaling error for the lower power limits as observable in Figure 4.4 which had to be taken into account in our final implementation. However, beyond this special case our initial tests revealed that with Equation 4.4 we could already derive a good estimate for the actuation time of a single spring contraction.

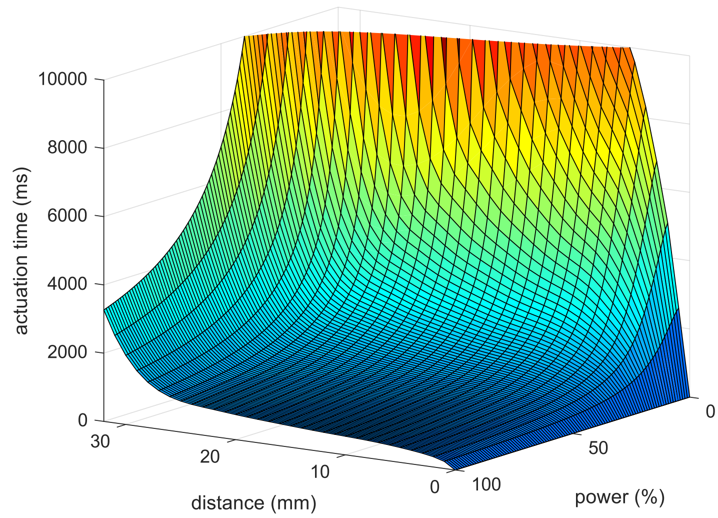

Figure 4.4: The *time-distance-power relation* for a single SMA spring actuation. Note that the power scale is inverted and the vertical axis describes the time interval limited to ten seconds for a proper visualization.

The model for a single SMA was extended for our two-dimensional approach involving two SMAs.

We incorporated this equation for a movement involving two active SMAs in a naive way. The movement distance d_i for the active SMAs was calculated in the same manner as described for the force equilibrium model. Assuming a movement is performed at maximum speed ($P_1 = P^*_{max}$), the actuation time t_b for the SMA with the larger required contraction distance d_1 is derived using the determined *time-distance-power* relation $t_b = T_{P_1}(d_1)$. Based on the actuation time of the first SMA we could then obtain a rough estimate for the required power level P_2 of the second SMA which has to perform the required contraction distance d_2 within the same amount of time $T_{P_2}(d_2) \stackrel{!}{=} t_b$.

The force decomposition is taken into account to model supportive and antagonizing behavior of two active SMAs.

We extended this basic approach to take into account that pulling the *tactor* by two SMAs may be of supportive as well as antagonizing manner depending on the movement. To derive a reasonable tuning parameter τ for the estimated time t_b, we aimed to take into account the force decomposition of $\vec{F}$ for the pulling force vectors $\vec{F_1}$ and $\vec{F_2}$ as illustrated in Figure 4.5. Assuming $F = 1$ and the angles α, β

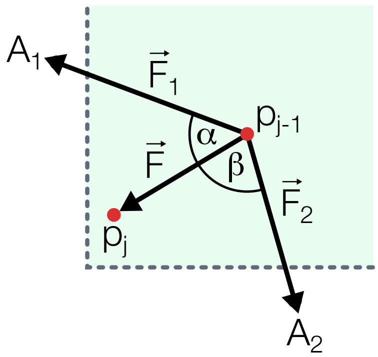

Figure 4.5: Parameters for obtaining the force ratio between two SMAs connected to the anchor points A_1 and A_2, assuming a boosted movement m_j is performed from p_{j-1} to p_j. Workspace area indicated in green.

are known, the force distribution can be calculated by the simplified formulas $F_1 = \frac{\sin\beta}{\sin\alpha+\beta}$ and $F_2 = \frac{\sin\alpha}{\sin\alpha+\beta}$. We then define $\tau = min(F_1, F_2)$ as our tuning factor for the estimated traveling time t_b of a boosted movement.

Discussion

This model allowed us to perform relative movements at a higher speed, predict the required time and furthermore control the speed of a single movement. However, as it only relied on rough assumptions and did not accurately model the occurring non-linear effects, small deviations of movements could easily accumulate and lead to an increasing targeting error for sequences of movements.

Coarse fast and timely controlled movements can be performed. Small errors can accumulate over time.

As the model moreover assumed that at least an initial *starting position* was known and the *force equilibrium model* allowed for more accurate target acquisitions, a dynamic approach comprising a mixture of both appeared to depict a reasonable next step.

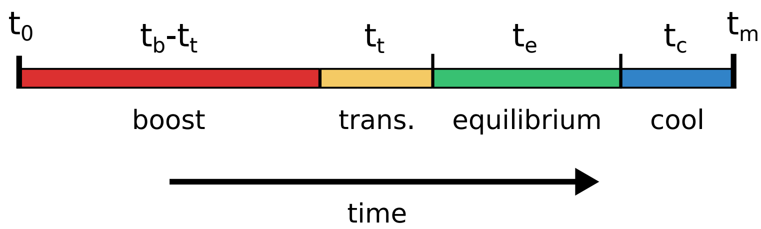

Figure 4.6: The four phases of the *hybrid model* for a single movement: *boost-*, *transition-*, *equilibrium-* and *cool phase*. t_0 describes the starting time of the individual movement. The total time for a movement is given by $t_m = t_b + t_e + t_c$. Note that the *transition phase* is part of the *boost phase* (t_b) but not of the *equilibrium phase* (t_e).

4.2.3 Hybrid Model

The *hybrid model* combined and extended our previously developed models in order to perform two-dimensional skin-drag gestures, consisting of sequences of movements, in a robust manner.

An initial calibration is performed at the center.

While an initial *calibration phase* was required anytime when a sequence of movements was supposed to be performed, each target position could be acquired in the same way afterwards. The *calibration phase* included a 'homing movement' towards the center point according to the *force equilibrium model* followed by a $10sec$ cool down. The center point C_0 was chosen to depict the homing position as a force equilibrium could be obtained most reliably by actuating all SMA springs at the same power level.

Slight deviations of coarse and timely controlled movements are corrected according to the *force equilibrium phase*.

Each subsequent target position was then acquired according to 4 phases as illustrated in Figure 4.6. First, a coarse relative movement was performed according to the *boosted movements model* within the *boost phase*. To prevent an accumulating error over time, the subsequent *equilibrium phase* aimed to correct slight deviations by applying the *force equilibrium model*. The combination of both allowed us to reduce our previously estimated required time of approximately $10sec$ to $2sec$ which appeared to suffice for consistent acquisitions. As our tests showed that the relatively hot active SMAs resulted in overshooting after rapid movements, we extended the *boost phase* with a *transition phase* with $t_t = 200ms$ at the end, whereby $t_t = t_b$ for $t_t \geq t_b$. Within the *transition phase* the non-active actuators were slightly preheated by continuously raising their power level to the required one of the following *equilibrium phase*.

A major problem still revealed to be the strong hysteresis effect which was not taken into account so far. In our two-dimensional case, the issue may be illustrated by imagining to repeatedly draw a circle using our proposed display design, whereby the SMA springs have to be actuated continuously in a clockwise manner. Due to the hysteresis effect of the material (subsection 3.2.2), the individual springs may not completely relax and result in a narrowing spiral. As the hysteresis and heat-transfer depicted two entangled effects which would be complex to model we, therefore, decided to introduced a *cooling phase* at the end of each movement. While we tried to dynamically adjust the time for this phase depending on the movement we finally decided to define a constant time of $t_c = 10sec$ which unveiled to be robust in order to assume that the same starting conditions would be given for the subsequent movement. The total movement time for a single movement was consequently given by $t_m = t_b + t_e + t_c$.

A cool down ensures to restore the initial starting conditions for the actuators.

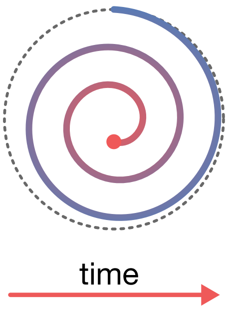

Hysteresis Spiral Problem

Discussion

Our final model depicted a compromise between the advantages and disadvantages of both (1) our *force equilibrium model* and (2) our *boosted movements model*. While (1) enabled us to acquire an arbitrary position within our workspace in an *accurate* and *consistent* way, we could perform *timely controlled* and *rapid movements* based on (2). With help of the *time-distance-power* relation derived for (2), we furthermore could adjust the *speed* and estimate the *traveling time* for a given movement. While the cool down of the SMA actuators would have had to be considered for any of the previous models, the constant amount of time $t_e + t_c$ which was added to each movement still revealed to be a

Sequences of movements can be performed robustly without a feedback loop. A constant amount of time is required for each movement.

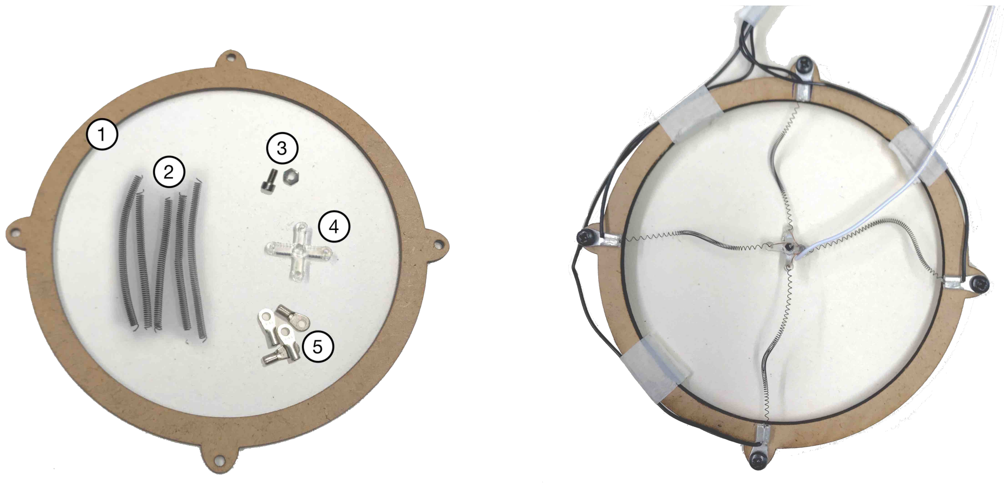

(a) (b)

Figure 4.7: **(a)** Essential assembly parts: (1) frame, (2) SMA spring actuators, (3) *tactor* (simple screw), (4) node mount, (5) ring terminals. **(b)** Top-view of the assembled two-dimensional actuator with electronic wires crimped to the SMAs

major drawback. Despite this, the model turned out to be robust to perform sequences of movements and, most importantly, afforded to realize a simple control system without a feedback loop.

4.3 Implementation

4.3.1 Display

The display can be easily fabricated and primarily consists of a simple *frame*, four *SMA springs* and a *tactor*.

The skin-drag display consists of five essential parts as shown in Figure 4.7a: a *frame*, *SMA spring actuators*, *ring terminals*, a *node mount* and a *tactor*. For the implementation we used the smallest version of the 90°C Flexinol® Spring Actuators [DYNALLOY Inc. 2019] with a *spring diameter* of $D_S = 1.37mm$ and a *displacement length* $L_D = 36mm$. The absolute *contraction length* $L_C = 25mm$ was experimentally determined by repeatedly actuating the SMA springs and steadily increasing the *displacement distance* until we reached a safe absolute of $L_E = L_C + L_D = 61mm$ (subsec-

Figure 4.8: A flexible version of the proposed skin-drag display attached to the forearm using kinesio tape and a rubber band.

tion 3.3.1). The *contraction force* of $40g$ revealed to be more than sufficient in order to drag a *tactor* across the skin and generate skin-drag sensations.

A cross shaped *node mount* with a diameter of $d_{node} = 14.366mm$ was cut out of $2mm$ thick acrylic glass using a $30W$ Epilog Zing laser cutter. It allowed to attach the individual SMAs and easily exchange the tactor. For our first version we decided to implement a planar and solid frame with a diameter of $2 \times r_{center} = 100.732mm$ using $3mm$ thick medium-density fibreboard (MDF). Four holes allowed to screw down *ring terminals* for the desired *anchor points*. As soldering would damage the spring actuators, they were crimped to the ring terminals along with electric wires and connected to a common node in the same way. Based on the given parameters we determined a workspace size of $32.16mm \times 32.16mm$ within which the tactor could be moved.

The device showed to be thin, but still revealed to have a large diameter. Kinesio tape was used to fix the display to the skin and protect it from heat.

For a second version of our display we printed a flexible frame using a Prusa i3 Mk2 3D printer and FilaFlex filament. To fix the skin-drag display properly on the user's skin we chose skin-friendly kinesio tape which was mounted to the frame with the help of double-sided tape. Holes for an exact alignment at the *anchor points* as well as a precise square for the workspace area were cut into the tape. This way, it furthermore provided a thermal isolation layer for the slight heat which was given off by the SMAs during actuation. Figure 4.8 shows the display fixed at the

A flexible frame allowed to align the device to the body's curvature. We still decided to use the wooden frame for the evaluation in order to validate our control model.

forearm. The flexible frame allowed to align the device to the body's curvature, while still providing a solid structure – due to its round form factor – to pull the tactor towards it. However, as the control model was developed based on the wooden frame, we did not use the flexible frame for the evaluation in order to be able to draw reliable conclusions on our control model.

4.3.2 Control System

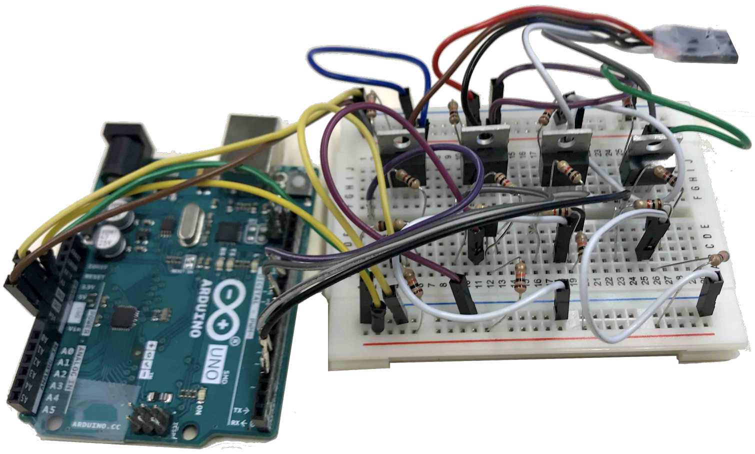

Figure 4.9: Breadboard with four gate drivers (MOSFET-drivers) and an Arduino UNO R3 as logic controller to control four SMA spring actuators. As the SMAs are connected to a common node, only five wires are required.

An Arduino UNO drives the SMAs according to the control model. A PWM signal is used to control four MOSFETs and feed the individual actuators with higher currents.

As we omitted a feedback-loop, we could break down our control circuit to a simple one (similar as described in subsection 3.3.3) which enabled us to drive four independent spring actuators at different power levels. An Arduino UNO R3 served as machine controller which could be connected to a computer via its serial port and interpret commands. To drive the SMAs at higher loads than supported by the logic unit, we used four IRF540 MOSFETs as power amplifier with a preconnected 2N2222A transistor as level shifter each. For safety reasons an additional 10k Ohm pull-up resistor was connected to the gate of the 2N2222A's to ensure that the SMAs would not be powered by default if the control unit is turned off. A detailed schematic can be found in Appendix B. To power the SMA actuators we connected a steady $9V$ DC power supply to the circuit.

DUTY CYCLE AND POWER VALUE:
Our setup allows us to control the actuation power for each actuator using pulse-width modulation, i.e. altering the fraction of time, power is supplied within a defined interval at a given frequency. This fraction is called *duty cycle* which is mapped to an unsigned $8bit$ value $(0-255)$ by the microcontroller. Depending on the context we may refer to the duty cycle in percentage or the mapped integer value (e.g. for our developed model). Otherwise we may report the resulting current value.

Definition: *Duty Cycle and Power Value*

The measured resistance of the SMA springs was 7.25Ω. We experimentally determined the control values by steadily increasing the power until we could (1) yield, and hold a force equilibrium for $10sec$ with a safe constant power for all SMAs, (2) obtain a fast and strong contraction ($40g$ pulling force) with a safe power value for a single actuator. Based on our estimations, we defined the PWM control value to a safe maximum of $P_{max} = 55$ (21.57% duty cycle, $237mA$) for our *equilibrium model* and an absolute maximum of $P^*_{max} = 90$ (35.29% duty cycle, $390mA$) for our *boosted movements model*.

We defined two maximum power values for the different model phases in order to ensure a safe operation of the actuators.

4.3.3 Machine Controller Interface

Similar to conventional machine controllers the Arduino UNO (ATmega328PU) of our control circuit (subsection 4.3.2) could be connected to a computer via USB and interpret commands being received at the serial interface. The gestures were then performed according to our developed *hybrid model* (see subsection 4.2.3).

Gesture Definition

So far, our actuation system did not provide dynamic control about the tactor beyond motion. A gesture was there-

Gestures consist of straight movements. For each movement a *movement time* can be specified.

fore performed by dragging the tactor along a predefined path consisting of straight movements as illustrated in Figure 4.10. Through the derived *time-distance-power* relation we could furthermore incorporate a rough control about the movement time as well as the average movement speed.

As the gestures consist of continuous movements, only the target points and corresponding movement times need to be specified.

A gesture could therefore be specified by a set of n successively acquired target points $p_i \in \{(x, y)|x, y \in [0, 32.16]\}$ within our workspace, $0 \leq i \leq n$. The movement m_j was indirectly defined by its starting point p_{j-1} and a target point p_j with $0 < j \leq n$. The *traveling time* t_j (in milliseconds) moreover depicted the time required to drag the tactor from the starting point p_{j-1} to the target point p_j for the jth movement.

As the skin-drag display would always perform an initial calibration at the center point $C_0 = (16.08, 16.08)$, the starting point for the first movement m_1 was given by default ($p_0 = C_0$) and each following point would describe a new movement. Consequently, only the target point p_j and an optional *traveling time* t_j had to be transmitted for the jth movement. When not specifying a *traveling time*, a movement was assumed to be performed at maximum speed.

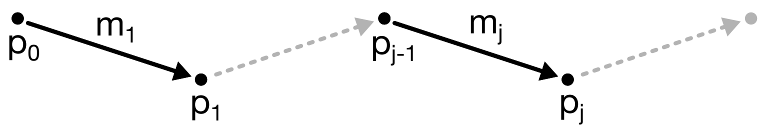

Figure 4.10: Movement Path

Command Interface

A gesture is transmitted in form of a batch job which is buffered by the controller and can be processed, i.e replayed, on demand.

A gesture could then be transmitted to the back-end using the commands listed in Table 4.1. The instructions were defined in human-readable code as no real time communication was required and it allowed for an independent testing by manually instructing the controller via a terminal. To keep the coordinates independent from the system size we furthermore decided to transmit normalized coordinates.

The controller received instructions via the serial interface in form of buffered commands. A machine controller instruction consists of a command character, optionally followed by a numeric argument and a $'new\text{-}line'$ as end-delimiter. Using the commands listed in Table 4.1 a gesture could be incrementally defined by adding a movement or cool down using $(4-7)$ with the (optionally) previously defined parameters through $(1-3)$. Plotting a gesture could be initiated using command 8. Command 9 resetted the system and cleared the sequence buffer. Hence, a gesture was treated in a similar manner to a job which is processed by conventional computer numerical control (CNC) machines.

System State and Feedback

Each successfully interpreted command was confirmed by a $'ok'$. While plotting a gesture the back-end reported the current system state in terms of which movement was going to be performed next as well as any power value change of the driven SMA actuators. Additionally, the start and finish of the complete process of plotting a gesture were reported via the serial interface.

#	Command	Argument	Description
1	X	normalized coordinate	*sets the x-coordinate for a target point*
2	Y	normalized coordinate	*sets the y-coordinate for a target point*
3	T	time in milliseconds	*sets the traveling time for a movement*
4	C	-	*adds a movement with params (X,Y,T)*
5	D	-	*adds a movement with params (X,Y,max)*
6	P	-	*adds a 10 seconds cool down*
7	p	-	*adds a cool down with time T*
8	S	-	*starts plotting the sequence of movements*
9	R	-	*resets and clears the movement list*

Table 4.1: Command Interface

Chapter 5

Design Tool

Next to the back-end of our skin-drag display we developed a graphical user interface (GUI) which allows to program our actuation system in an easy way. Our target user group depicted researchers who seek to explore diverse on-skin gestures for different contexts. We therefore intended to provide a tool which resembles the device properties in a realistic way and make physical boundaries of our skin-drag display as well as constraints of the supported gestures obvious to the user. The user should be able to 'play around' and easily figure out these limitations while being capable to accurately control different parameters.

5.1 Design Tool Components

The graphical user interface can be split into four major parts (see Figure 5.1). The *movement area* was supposed to provide the user with an intuitive visual representation of the two-dimensional workspace and already allow to design the movement path in a simple and coarse manner. The *movement list* was intended to provide an overview about the sequence of movements. Properties such as the position and speed of a selected movement could be specified in a more accurate way in the *movement settings* part. At the bottom an additional *status bar* reported about the

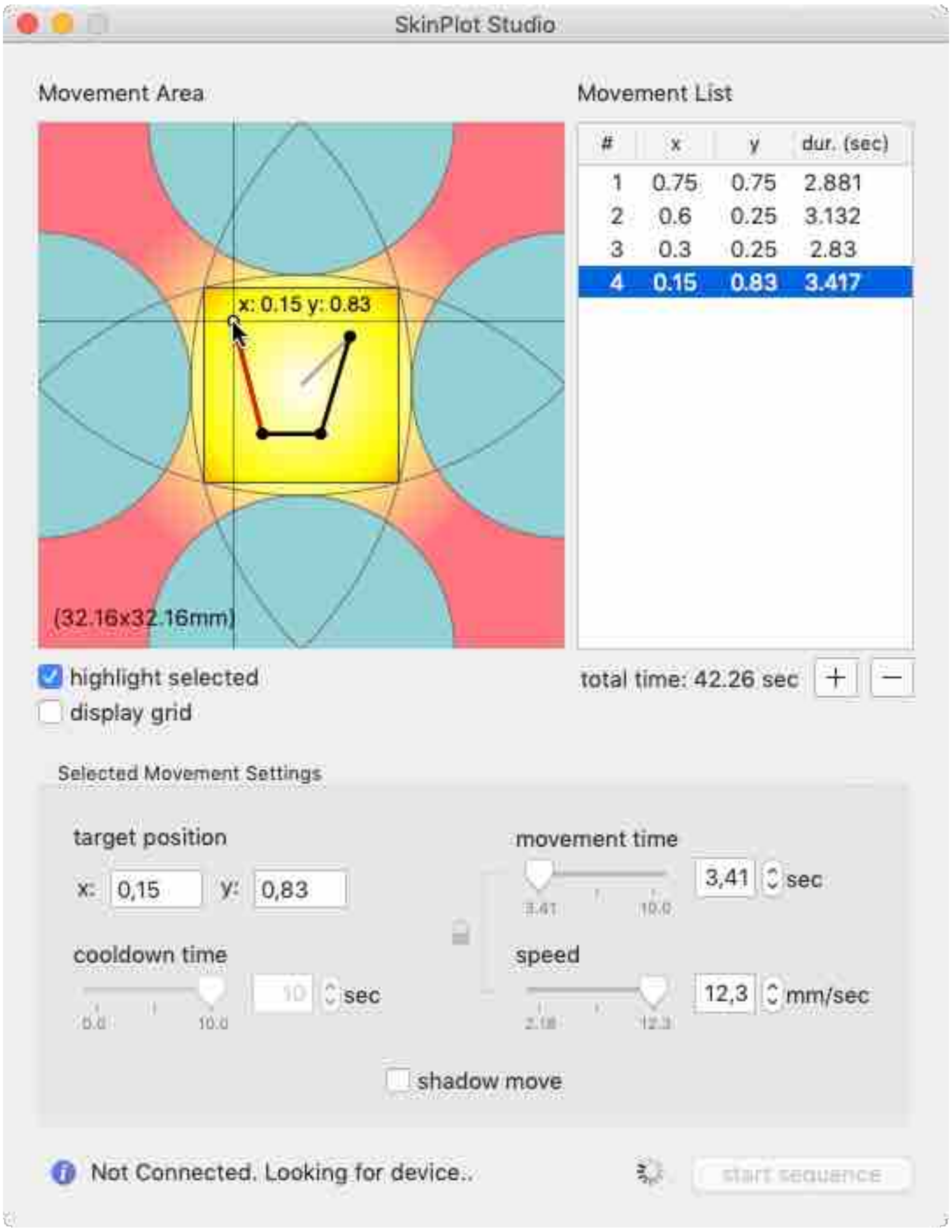

Figure 5.1: Gesture Design Tool: The graphical user interface allows to design, save, load and replay skin-drag gestures. It can be split in four major parts including the *movement area*, *movement list*, *movement settings* and *status bar*.

current system state of the back-end. However, feedback from the back-end (section 4.3.3) such as the currently performed movement were also indicated graphically in the user interface.

5.1.1 Shadow Movements

Although the dragged tactor would cause a tactile sensation for any movement as it had continuous contact to the skin, we believed that a future system would allow for turning the stimulus on and off. Hence, we introduced the concept of *shadow movements* for our high level abstraction of the programming interface. A user should be able to come up with gestures which may yet not be supported, i.e. design a movement path which includes unwanted movements. We call movements which are not intended to be part of the gesture '*shadow movements*'.

As the tactor applies continuous pressure, the user is able to mark unintended movements as *'shadow movement'*.

The user could therefore mark movements which are not intended to belong to the gesture as *shadow movement*. Marking a movement, however, did not have any impact to the actually performed gesture. *Shadow movements* were only visually indicated in the *movement area* view as gray lines. As the initial movement always starts at the center and was considered to depict an unintended movement in most cases, we decided to mark the first movement as *shadow movement* by default (see Figure 5.1).

So far, marking a movement only affects the gesture representation in the GUI.

5.1.2 Cool Down

Initially we aimed to provide the user with control about the time for the *cooling phase* after a movement. Our assumption was that if we could roughly model the hysteresis effect and heat transfer, we could try to estimate to which degree the effective movement area for the subsequent movement would shrink and allow the user to place the next end-point within this area. As this unveiled to be more complex and decreased the stability of our open-loop control model, we decided to disable this feature for our

Temporally reducing the cool down may be a desired feature, though it affects the SMAs behavior. We decided to disable the UI component for now, to ensure a robust operation.

user study and maintain a safe operation of the actuation system. The cool down time was therefore fixed and set to ten seconds.

5.2 Gesture Design

The design of a gesture could be performed offline, i.e. without having the skin-drag display connected to the computer. As described in section 4.3.3, a gesture was mainly defined by its *movement path* depicting a set of subsequently acquired *target positions*. For each movement the *movement time* (or 'traveling time') could be specified. We furthermore introduced the speed of a movement as an additional parameter which may be of interest. The cool down time was fixed. Optionally a movement could be marked as *shadow movement*.

5.2.1 Defining the Movement Path

A user could design the movement path in a similar manner to that of common vector graphic applications. As discussed before, the starting point of the first movement was always set to the center point because of the initial *calibration phase*. Adding a node to the movement path would therefore describe the *target position* for the subsequent movement.

The movement path can be defined by adding, clicking and dragging nodes which describe the target points of a movement.

Hence, a movement could simply be added to the sequence by left-clicking at a desired target location in the *movement area* or pressing the plus-button below the table-view. For the latter, the target position would depict the center point by default. In a similar fashion a selected movement could be deleted, by either right-clicking or pressing the minus-button. A movement could be selected by clicking on the according row in the table-view or at the node in the *movement area*. The current selection was indicated by the highlighted row in the table view and graphically represented as a red line in the *movement area*. A node could be dragged across the workspace to change its position and alter the movement path on the fly. For more precise input a grid could be toggled which served as visual reference or the normalized coordinate could be entered directly using the input fields in the *movement settings* section.

5.2.2 Time and Speed Control

By default a new movement was performed at maximum speed, i.e. with the lowest movement time. Next to the the movement time, the speed parameter should provide the designer with the ability to adjust or align the speed levels of different movements. The speed parameter only depicted a rough estimate for the distance (mm) per time (sec). We indicated the boundaries below the sliders to make the user aware of the possible range for a given movement. We defined a maximum movement time of ten seconds as well as a minimum time of two seconds due to the *equilibrium phase*. The speed was simply calculated by taking the movement distance and dividing it by the movement time (excluding the two seconds for the *equilibrium phase*. Increasing the movement time would decrease the movement speed and vice versa. To make the relationship easy for the user to discover, we indicated the dependency of both parameters visually with a 'lock symbol' which is a common metaphor used for uniformly cropping and scaling images. In addition, the slider controls and displayed values updated immediately on any change of the parameters - making the relation even more obvious during interaction.

Next to the *position*, the *movement time* and *speed* for each movement can be set. The dependencies between the parameters are made obvious.

5.3 Plotting a Gesture

To test and plot a gesture using the skin-drag display, it had to be connected via USB. The interface automatically recognized if the skin-drag display was connected to a serial port which was reported at the status bar along with enabling the 'start sequence' button. On pressing the button, the sequence data would be transmitted to the controller as described in section 4.3.3 and the machine controller would be triggered to start plotting the sequence using the corresponding 'start sequence' instruction. While the user interface did not simulate and visualize the continuous movement of the tactor the user could monitor the progress based on the table view and movement area, which highlighted the currently performed movement based on the received status information at the serial port. In addition, the current progress as start, finish and the current movement number was reported in the status bar.

Chapter 6

Evaluation

The proposed system was evaluated in two ways: First, the skin-drag display was evaluated regarding positional accuracy and its gesture plotting performance in a technical way (section 6.1). Secondly, a small user study was conducted in order to validate the on-skin perception of our device in a preliminary way (section 6.2) and test our design tool with respect to its usability (section 6.3).

6.1 Technical Evaluation

With our technical evaluation we aimed to answer four major questions regarding our proposed apparatus:

Q1: How accurately can targets be acquired within the defined workspace?

Q2: Can single target acquisition as well as sequences of movements be reproduced consistently?

Q3: Does our open-loop system decrease in accuracy over time for sequences of movements?

Q4: How well do the plotted shapes match the intended design?

We sought for answering these questions within two separate tasks. With our target acquisition task we wanted to address (Q1) and (Q2) by repeatedly acquiring different targets from the the center. With the sequence of movements task we aimed to answer (Q2-Q4) by plotting different shapes consisting of straight lines.

6.1.1 Apparatus and Setup

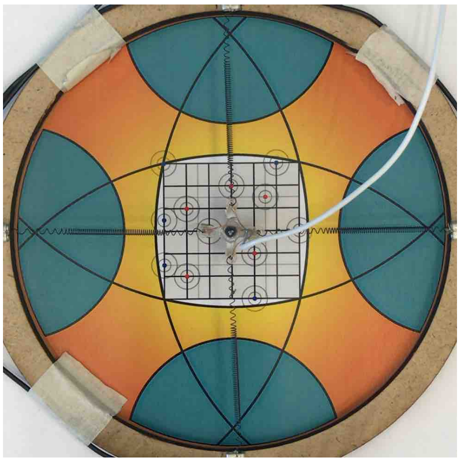

Figure 6.1: Top view of the prototype used for tracking the operation point. The snapshot shows the system during the *calibration phase* at the center. The printout placed below the actuator shows the target points within the workspace area.

The *operation point* was visually tracked from the top using a camera.

The tests were performed in a controlled environment with minimized airflow at a constant room temperature of $26°C$. An iPhone 7 was used in order to take video recordings (1080×1920 pixels, 30 fps) of the skin-drag display during the tasks. The smartphone was mounted on a tripod with the camera horizontally aligned to a parallel plane above the actuator.

The solid frame was used in order to validate the control model under the same conditions it had been developed on.

The skin-drag display was fixed on a table using tape. We decided to use the same solid and wooden frame for the evaluation which had been used in order to derive our control model. In order to track the *operation point* and take accurate measurements afterwards, we attached a printout to the bottom of the two-dimensional actuator displaying the estimated workspace including the target points on a predefined grid. The screw tactor was replaced by a tiny metal needle which could be tracked more accurately. A snapshot of the camera view is shown in Figure 6.1.

6.1.2 Design and Procedure

Target Acquisition Task

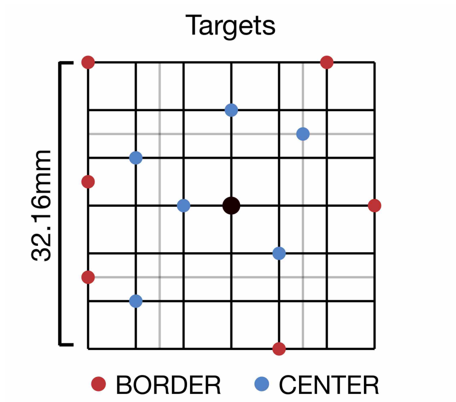

Figure 6.2: Selected target points within the workspace area: 6 points at the border B1-B6 in red; and 6 contained points C1-C6 in blue (enumerated from left-right, top-bottom).

We assigned a 6×6 grid to our workspace ($32.16 \times 32.16mm$) from which we chose 12 different target points as shown in Figure 6.2. Intermediate steps as for C2 and B3 were considered, too. The target points were carefully selected in order to represent *unique features* on the predefined grid, and being *equally distributed* across the workspace at the same time. We ensured that no point would be represented by another point mirrored by any of the workspaces' symmetry axes. The targets were, furthermore, divided into two groups. Six target points at the BORDER (B1-B6) and six contained target points around the CENTER (C1-C6).

Twelve individual target points were repeatedly acquired to investigate on accuracy and consistency.

Each target target was acquired three times resulting in $12 \times 3 = 36$ trials in total. For each trial, the actuator

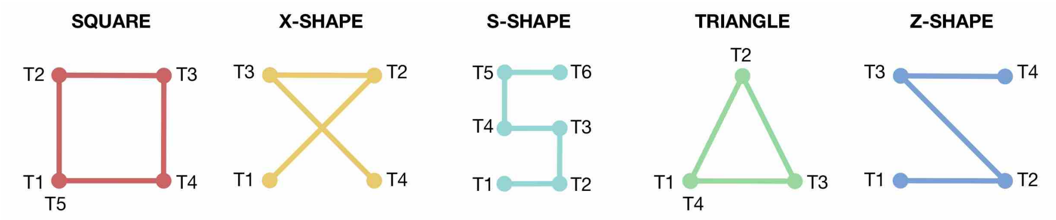

Figure 6.3: Selected shapes with labeled target point numbers for the sequence of movements task. The initial *shadow movement* from the center to target T1 is omitted.

first calibrated at the center point C_0, followed by a $10sec$ cool down, before approaching the target point at maximum speed based on our developed control model (subsection 4.2.3). The end of the target acquisition was indicated by a short LED flash. After another $10sec$ cool down it was continued with the next trial. Targets were acquired in randomized order.

Sequence of Movements Task

Five different shapes were repeatedly plotted to investigate on robustness over time and shape matching performance.

For the sequences of movements we chose five simple shapes which were also supposed to be used in the perception study shown in Figure 6.3. A SQUARE, TRIANGLE, X-SHAPE, Z-SHAPE and S-SHAPE. The Z-SHAPE was mirrored and the S-SHAPE plotted from bottom to top as we obtained the same initial *shadow movement* for each shape this way. The shapes were plotted in the order as presented in Figure 6.3 (left to right). Similar to the target acquisitions, each shape was plotted three times resulting in $3 \times 5 = 15$ trials in total. Here, one trial denotes one sequence of movements. Considering the different numbers of target points, the total number of data points sums up to $(5+4+4+4+6) \times 3 = 69$.

Before conducting the tests, the SMA spring actuators were actuated more than 100 times.

6.1.3 Measurements

For each target acquisition the position of the effectively reached point was measured based on pixel points. These were put in relation to the workspace dimension to derive distance values in millimeters. For the sequence of movements task we used a motion tracking tool[1] in order to trace the performed movements of the individual shapes. To investigate on time dependent effects and systematic errors we introduced three measurements: The *targeting error*, the *adjusted targeting error* and the *center error*. The analysis of the data sets was performed using common correlation and linear regression methods. Pearson and Spearman correlation methods were used in a supportive manner to discover potentially hidden effects by looking at the pairwise relation of diverse variables including *target position*, *group*, *order*, *repetition*, *direction (diagonal/horizontal/vertical fraction)*, *center distance*, *axis wise difference*, *targeting error*, *standard deviation*, the *adjusted targeting error*, *average deviation* and the *center error*. The *shape*, *target point number* and *movement length* were additionally taken into account for the sequence movements task. Statistical significance was mainly used in a supportive manner and not considered in a strict way.

The relation of diverse variables was taken into account within the analysis. Two additional error measurements were introduced to allow for investigating on effects independent from a systematic error.

TARGETING ERROR:
The *targeting error* depicts the distance between the defined *target point* of a movement and the measured *effectively reached point* in millimeters (mm).

Definition: *Targeting Error*

CENTER ERROR:
The *center error* is defined as $\frac{d_{ct}-d_{cm}}{d_{ct}}$, whereby d_{ct} depicts the distance between the center point and the target point; and analog for the measured point for d_{cm}. By normalizing the value we aimed to get a robust measurement which would allow us to detect accumulating effects such as hysteresis or fatigue of the SMAs over time.

Definition: *Center Error*

[1] https://physlets.org/tracker/

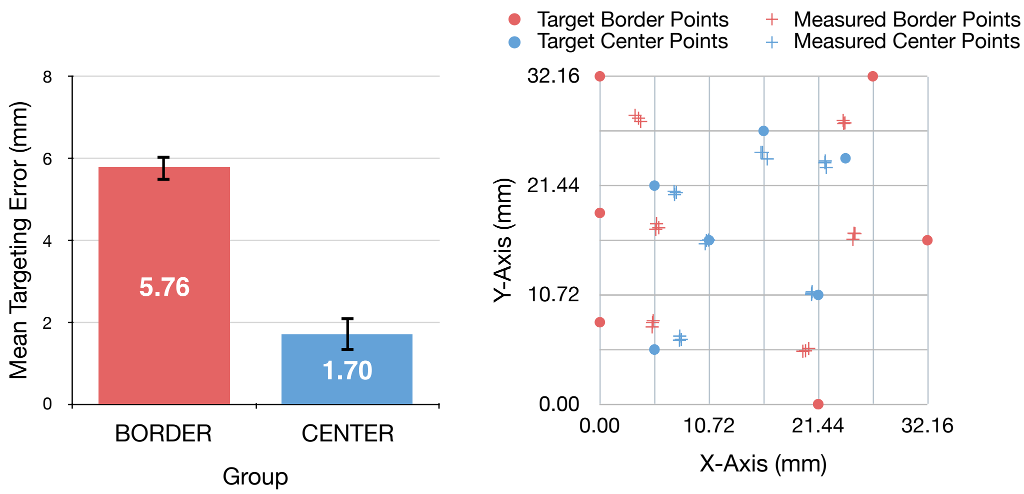

Figure 6.4: The BORDER group shows a significantly higher mean targeting error compared to the CENTER group (error bars show the standard error) (left); The measured points indicate a systematic error, border points are barely reached from the center (right).

Definition: *Adjusted Targeting Error*

ADJUSTED TARGETING ERROR:
The *adjusted targeting error* is defined by the distance of a measured point to the centroid of all measured points for the same target acquisition (in millimeters). It would therefore take into account a potential systematic error. The mean of the *adjusted targeting error* was furthermore considered to depict a more robust value for the *average deviation* of repeated target acquisitions.

6.1.4 Results and Discussion

Individual Target Acquisitions

On average, the targets were reached with a mean targeting error of $M = 3.73mm$ ($SD = 2.28$). The targeting error for the BORDER group B1-B6 depicted $M = 5.76mm$ ($SD = .75$); CENTER points C1-C6 performed significantly better with a mean targeting error of $M = 1.70mm$ ($SD = .99$) (Figure 6.4, left). The relatively low standard deviation, suggested a good consistency for repeated acquisi-

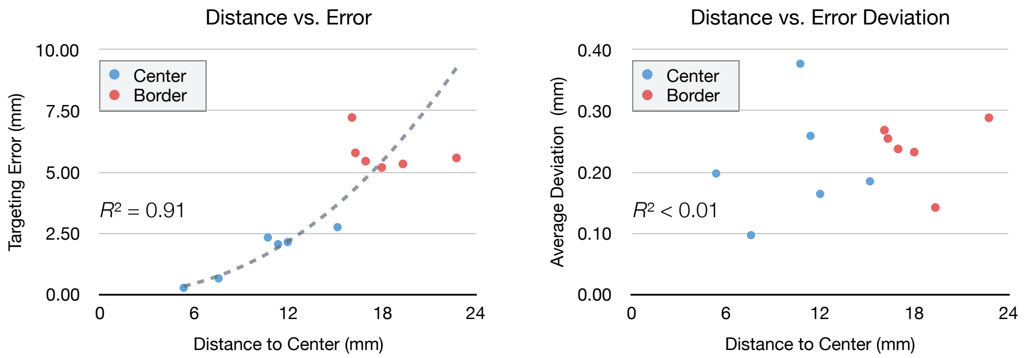

Figure 6.5: The average *targeting error* for the individual targets increases with the distance from the center (left). The low *average deviations* show to be uncorrelated to the distance from the center (right).

tions which indicated a systematic error. Plotting and comparing the intended targets with the measured points (Figure 6.4, right) appeared to support this assumption. Targets at the border unveiled to be barely reached at all, suggesting that the EMA had decreased.

The accuracy decreased with increasing distance from the center. The *targeting error* deviated little for repeated target acquisitions.

While we could not determine an increasing error over time, the *targeting error* as well as the *center error* showed to increase with the distance to the center. The average *targeting error* for the individual targets was found to be strongly positively correlated with the targets' *distance to the center*, $r(10) = .86, p < .001$. In addition, the average *center error* for the individual targets was found to be strongly positively correlated with the targets' *distance to the center*, $r(10) = .72, p < .01$. By further investigating on the *center distance* and *targeting error*, we could infer a non-linear relation described by a power-curve fitting to CENTER as well as BORDER targets as shown in Figure 6.5 (left, $R^2 = .91$). As the *average deviation* of repeated target acquisitions does not show to correlate with distance to the center (Figure 6.5, right, $R^2 < .01$), it supports the assumption of a systematic error described by the power-curve. The low *average deviation* furthermore indicates a strong consistency regarding repeated target acquisitions.

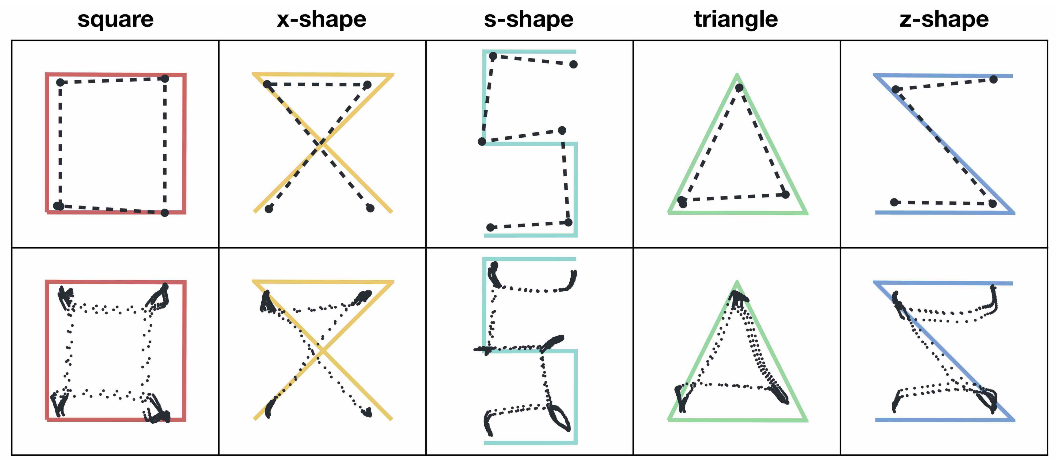

Figure 6.6: Comparison of the plotted shapes (black) and the intended shapes (color coded). The top-row shows the mean of the reached target points connected by straight lines (dashed); the bottom row shows the tracked points comprising all repetitions of the corresponding shape.

Sequences of Target Acquisitions

The mean *targeting error* of all target acquisitions for the sequences of target acquisitions depicted $M = 2.08mm$ ($SD = .67$). The mean targeting errors of the individual shapes are listed in Table 6.1. *Movement length* and average *targeting error* showed a strong positive correlation, $r(21) = .64, p < .01$. Also the targets' *x-coordinate* was found to positively correlate with the average *targeting error* of multiple target acquisitions, $r_s(21) = .42, p < .05$. By investigating on the individual actuators we found that the right actuators' pulling strength was weaker compared to the others. The reduced pulling force furthermore could explain the non uniform scaling, in particular observable for the target points at the right of the SQUARE and Z-SHAPE (Figure 6.6). As diagonals mainly described longer movements which were performed from left-to-right, this may also explain the increased error for longer movements.

The SMAs' behavior appeared to have converged to an equilibrium introducing the systematic error.

The average *targeting error* did not show to increase over sequences of movements. However, a positive correlation of the overall *acquisition number* and the *center error* was found, $r_s(21) = .49, p < .05$. By investigating on four target points

shape	mean error (mm)	SD (mm)
SQUARE	1.93	.62
X-SHAPE	2.31	.58
S-SHAPE	1.39	.59
TRIANGLE	2.20	.68
MIRRORED-Z	2.57	.33

Table 6.1: Shape Targeting Errors

(T1-T4 of the SQUARE, commonly shared by most shapes, $N = 48$) we could observe a slight increase of the *center error* by about $1mm$. A second degree polynomial showed to explain the relation best ($R^2 = .35$). Its decreasing slope indicated that the SMAs actuation performance converged to an equilibrium and the EMA would not decrease much further.

To obtain a direct comparison between the traced movements and the intended shapes we plotted both in individual charts (Figure 6.6). The *cooling phase* showed to have a strong adverse effect on the subsequent movements: The tactor unveiled to drift towards the center on the flat surface during the cool down, resulting in an offset for the starting point of the followed movement. Figure 6.7 illustrates the effect of the cool down exemplary for the SQUARE shape. Assuming the movement starts at the same endpoint as measured during our test, the same movement paths would resemble the target shape significantly better.

While subsequent movements were affected by a deformation during the cool down, the targeting error did not show to increase over time.

6.1.5 Conclusion

ACCURACY (Q1): The estimated workspace showed to have shrank to about $22.16mm \times 22.16mm$ after more than 100 actuation cycles. Consequently, the control model, being tailored to the larger EMA, introduced a systematic error with respect to the targets distance to the center. The sequence of movements task, indicates that targets can be acquired sufficiently well within a smaller workspace area, $M = 2.08mm$ $(SD = .67)$. The small deviations of repeated target acquisitions suggest that the targeting error can be significantly reduced by taking into account the systematic

The EMA had decreased and introduced a large error for border points. Within a smaller area, targets could be acquired accurately.

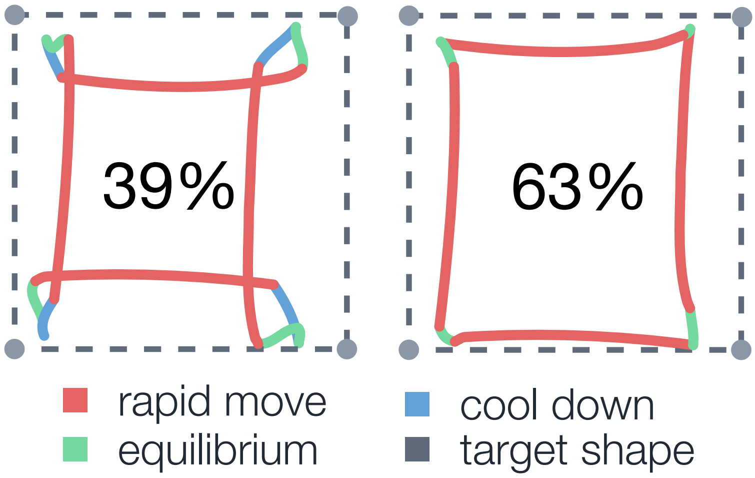

Figure 6.7: The plotted SQUARE shape is affected by the cooling deformation (left, blue); the same rapid movements and effectively reached positions without the cooling deformation result in a better shape matching (right): The fraction of the enclosed area of the plotted square increases from 39% to 63%.

error for the control model.

The small deviations of repeated acquisitions suggest that taking into account the systematic error could lead to high accuracy.

CONSISTENCY FOR REPETITIONS (Q2): The skin-drag display showed to be able to acquire targets very consistently for both of the tasks. Despite the tactor drifted towards the center during the *cooling phase*, the *equilibrium phase* appeared to correct the deviations and prevent an accumulating *targeting error* for sequences of movements. As the S-SHAPE reveals, the system even appeared to be able to recover from larger *targeting errors*.

ROBUSTNESS OVER TIME (Q3): Although, the workspace showed to have shrank after more than 100 actuation cycles, the *targeting error* did not increase significantly over time and the *center error* indicated that the implemented SMA actuators performance converged towards an equilibrium. The constant cool down time of $10sec$, appeared to afford a stable operation for sequences of movements.

SHAPE MATCHING (Q4): By looking at the reached target points (Figure 6.6, top) the proposed system unveiled to be capable of resembling the intended shapes in general. However, the movements still show larger deviations from the intended ones (Figure 6.6, bottom). Without a quantitative measurement, shape matching showed to be moderate-low. The *cooling phase* clearly introduced a larger error for subsequent movements and depicted the most critical factor with respect to the shape matching performance.

Even though the cooling deformation had a major impact and decreased shape matching, the model showed to be robust over time.

While a closed loop control system would certainly be able to overcome most of the problems, our developed open-loop control system already showed to perform good and afford a high consistency regarding repeated target acquisitions.

6.2 On-Skin Perception

Even though our two-dimensional actuator was not optimized for wearability, we aimed to validate its perception in a preliminary way to identify major design issues for potential future improvements.

Within a shape recognition task we investigated on the comfort and noticeability of our proposed system by varying the speed of five distinct skin-drag gestures, i.e. shapes.

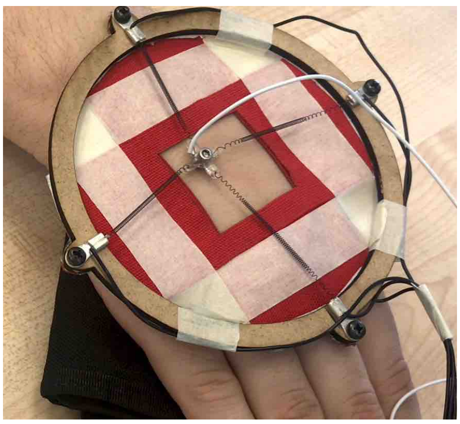

Figure 6.8: Skin-drag display mounted on a users hand performing a gesture.

6.2.1 Setup

The solid frame was fixed to the user's back of the hand with the help of kinesio tape.

To ensure that the gestures would be performed in the same way as tested before, we decided to keep the solid wooden frame for our preliminary user study, too. The kinesio tape allowed to fixate the display on the users skin and could easily be exchanged after a user's session.

Since Caswell et al. [2012] let suggest that the back of the hand is similar sensible to skin-stretch and motion stimuli as the forearm we chose to test our device at the back of the users hand (Figure 6.8). The back of the hand provided us with a larger fixation area and increased the stability of our planar two-dimensional actuator. A cushion aimed to allow for a relaxed finger position. An iPhone 7 was used to take video recordings of the actuator and user's hand during the sessions similar to the technical setup (subsection 6.1.1).

6.2.2 Gesture Selection

The same shapes as for the technical evaluation were evaluated regarding perceptibility.

We used the same shapes as for the sequence task of the technical evaluation (Figure 6.3): a SQUARE, TRIANGLE, Z-SHAPE, X-SHAPE and S-SHAPE – five shapes in total. The shapes were chosen to be simple, with a preferably similar total movement time, path length and shape complexity. Although the S-SHAPE constituted a special case, we decided to keep it as reference for the evaluation. The *shadow movements* were considered to be part of the gestures, excluding the initial movement from the center point. It was paid attention to design the movement paths, such that the shapes would share a common starting point at the bottom-left corner.

6.2.3 Design and Procedure

At the beginning the participants were supposed to fill out a demographics questionnaire regarding age, gender, their experience in programming and haptics design. To derive a rough estimate for the participants hand size, the contours were marked on a piece of paper. The number of hairs within $1cm^2$ at the center of the back of the hand were count to obtain a value for the individual hair density.

The users could only feel the gestures at the back of their hand. A sleeping mask prevented them from visually perceiving the system state.

The participants were asked to sit in front of a table with the dominant hand resting comfortably on a small cushion – affording a relaxed finger position. During the session participants wore a sleeping mask to prevent them from visually perceiving the actuators' state. The subjects were asked to keep their head straight facing in the direction of their hand and arm, which were resting on the table. The actuator was fixed on the back of the user's hand with the y-axis aligned to the straight hand orientation, facing away from the user.

Each user had to recognize five shapes at three different speed levels. In addition, the participants were interviewed regarding noticeability, confidence and comfort.

The gesture recognition task consisted of five blocks. In each block one of the gestures was plotted at three different speed levels (fast, slow, varying). Consequently each block consisted of three trials. For each trial the participants were asked to describe what they felt and whether they recognized one of the gestures including the option 'None'. They were furthermore supposed to rate the noticeability and comfort of a gesture, as well as their confidence of identifying the correct shape on a 5-point Likert scale (1 lowest - 5 highest). After the initial trial the subjects were additionally asked whether the performed gesture was perceived to be slower, faster or equal compared to the speed of the preceding trial (Appendix D).

The gestures were visually presented to the participants before a session including *shadow movements*. The subjects were told that in each trial either one or none of the presented shapes may occur and at different speed levels. They were asked to think aloud and describe what they feel during each trial. A beep indicated the start and end of of a gesture for each trial.

After the session the participants were supposed to fill a questionnaire regarding the overall perception of the device:

- How noticeable was the actuator on average? (1-5 Likert scale)

- How comfortable was the actuator on average? (1-5 Likert scale)
- How distinguishable were the shapes between the blocks? (1-5 Likert scale)
- Did you find some shapes be more distinguishable than others? If so, please describe which and why. (open)
- How well could you feel when a shape was slowed down or sped up? (1-5 Likert scale)
- Did shape speed influence perception? If so, how? (open)
- Did shape speed influence distinction? If so, how? (open)
- Did shape speed influence comfort? If so, how? (open)

The blocks were counterbalanced using a Latin Square and the speed levels randomized within the individual block.

5 SHAPES $\{$SQUARE, TRIANGLE, MIRRORED-Z, X-SHAPE, S-SHAPE$\}\times$ 3 SPEEDS $\{$FAST, SLOW, VARYING$\}$ $\times$ 5 REPITITIONS $=$ $75 samples$

6.2.4 Participants

Overall, 5 participants (2 female, 3 male) were recruited aged between 20 and 45; all right-handed. The average hand size was $M = 34.59cm^2$ ($SD = 11.11$). Female participants showed to have a glabrous skin at the back of the hand. The hair density for the male participants depicted $M = 9.33cm^{-1}$ on average ($SD = 2.52$). All users had experience with GUI design. Three stated that they were familiar with programming embedded systems. All but one participant stated to have experience with haptic interfaces (3 as developer).

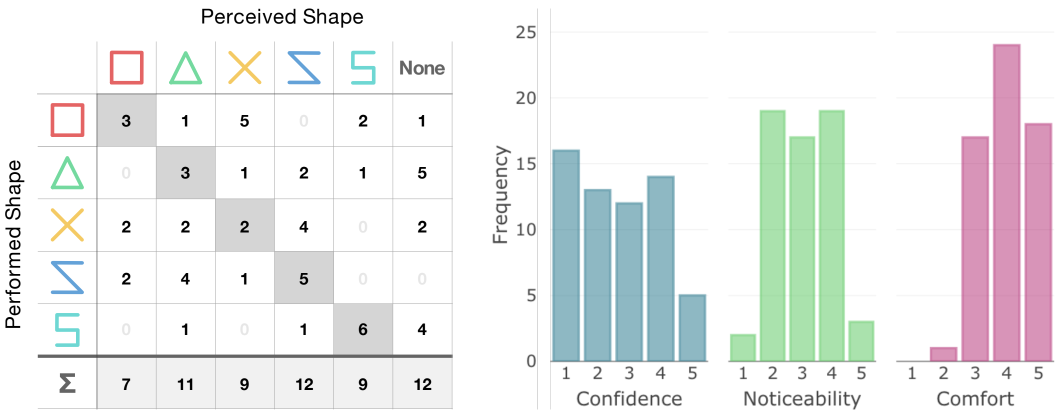

Figure 6.9: Shape confusion matrix (left); Subjective rating frequencies for all trials on a 5-point Likert scale (right, 1 very low - 5 very high).

6.2.5 Results and Observations

Although our pilot test appeared to be promising, the gesture perceptibility within our preliminary user study still revealed to be low. We decided to drop P1 as she encountered multiple problems and stated to barely perceive the tactor. It was noticed that the tactor sometimes hovered above the skin. This appeared to be caused through the hands slope at the right side. In accordance, the confidence rating of P1 was very low and in 12 of 15 cases 'None' was selected as perceived shape. Only one shape was selected correctly with low confidence. In each case the user answered that the speed level was equal.

We will therefore briefly report the raw results omitting P1 and focus on the qualitative evaluation by looking at different observations and statements from the individual participants.

Overall Results

Without P1 19 of 60 shapes were identified correctly which increased the gesture recognition rate slightly from 26.67% (including P1) to 31.67% (excluding P1). P2 and P4 identified a correct shape most often (7 and 6 times respectively);

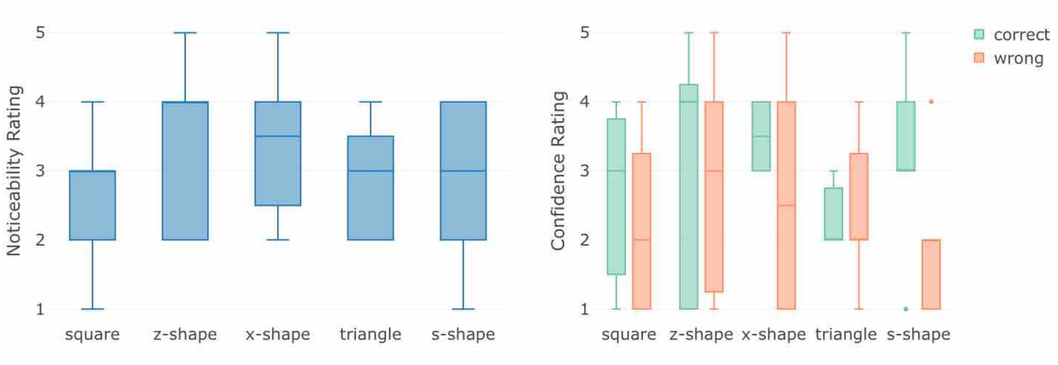

Figure 6.10: Noticeability and confidence ratings by shape on a 5-point Likert scale (1 very low - 5 very high): Overall the Z-SHAPE showed to be most noticeable (left); users appeared to be slightly more confident for correct answers – in particular regarding the S-SHAPE (right).

P3 and P5 3 times. While dropping P1 increased the median from 2 to $Mdn = 3$ (1 very unconfident - 5 very confident) for the overall confidence rating, participants still revealed to be very unconfident in many cases and answered that they could not identify any shape in 12 of 60 cases (see Figure 6.9). Noticeability of the performed gestures was rated to be moderate with $Mdn = 3$. Comfort was rated high ($Mdn = 4$). The S-SHAPE (6 times) and Z-SHAPE (5 times) were identified correctly most often. The X-SHAPE was perceived least often (2 times).

Shape Related Results

Users tended to be unconfident in general; the triangle showed to be most confusing.

While no significant difference between the means of wrong and correctly answered shapes could be found, Figure 6.10 indicates that for most shapes users tended to be more confident if the shape was perceived correctly. Despite the X-SHAPE was perceived least often, users showed to most unconfident regarding the TRIANGLE, even if the shape was identified correctly ($Mdn = 2$). In contrast, the subjects were clearly more confident when identifying the S-SHAPE correctly ($Mdn = 3$, distinct quartiles). The quartiles of the Z-SHAPE showed stronger varying confidence for correct answers while still revealing the highest confidence rating ($Mdn = 4$). The medians regarding the notice-

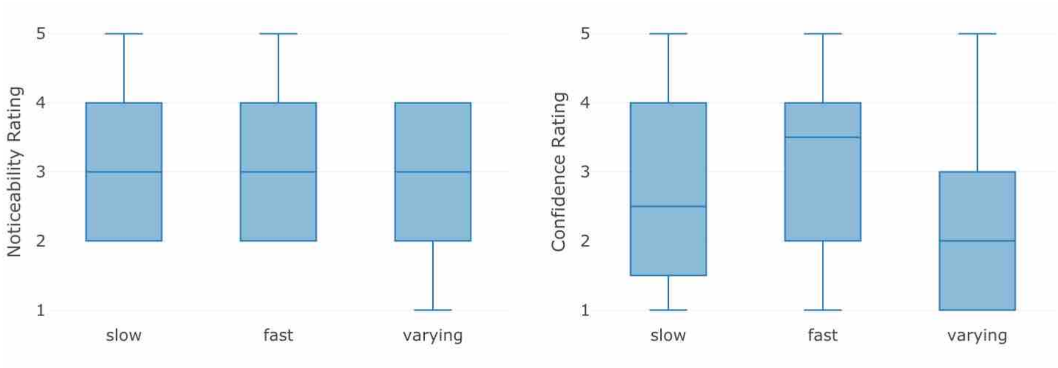

Figure 6.11: Noticeability and confidence ratings regarding different speeds on a 5-point Likert scale (1 very low - 5 very high).

ablitiy show to follow the ranking of the medians of the user's confidence for correct answers, but the TRIANGLE (Figure 6.10). Z- and X-SHAPE showed to be most noticeable with $Mdn = 4$ and $Mdn = 3.5$ respectively. The comfort of the different shapes was rated similar high $Mdn = 4$. Only the Z-SHAPE revealed a slightly higher median value of $Mdn = 4.5$ compared to the other shapes.

Speed Related Results

The comfort regarding the different types of speed were rated equally high with a median of $Mdn = 4$. While the noticeability revealed to be rated equally across the different speed types with a moderate rating of $Mdn = 3$, users showed to be more confident if the gestures were peforemd at fast speed $Mdn = 3.5$. Regarding slow gestures, users rated the confidence to be lower with $Mdn = 2.5$ and $Mdn = 2$ for gestures varying in speed. Slow gestures were correctly identified 4 times, fast ones 9 times, and gestures with varying speed 6 times.

Though users were more confident regarding fast shapes, slow shapes were identified twice as often.

6.2.6 Observations and Discussion

During the sessions, several issues became obvious. At first, it should be noted that recognizing the correct di-

The tactor was noticeable but the direction hard to recognize.

rection already revealed to be hard for the participants. Especially diagonal movements were rarely recognized and 'easily confused with simple horizontal or vertical' (P3). P5 only perceived horizontal movements for the diagonals of the triangle shape. The diagonals of the triangle unveiled to introduce most difficulty which is reflected by the users confidence rating and comparable high number of answers depicting 'None' (5 times, see Figure 6.9).

The cool down time added to the mental load. Users were tempted to take on a think-pose.

The cool down time of $10sec$ between the movements, showed to increase complexity and add to the mental load of the participants by interrupting the gestures for a comparable long fraction of time. Without any reference points it unveiled to be hard to follow the relative movements belonging to the different shapes. Users were tempted to take up a typical 'think-pose' and appeared to reconstruct performed movements mentally, trying to match them to one of the proposed shapes. If a movement was perceived differently as expected, their mental model seemed to break down and sometimes introduced complete confusion; often followed by the sentence like 'that does not make sense at all' (P2) or 'no shape could match these movements anymore' (P4). Changing the body posture furthermore may have lead to increased misconceptions regarding the direction. As the subjects were blinded their mental mapping of the movements and the hands coordinate system may have been prone to drift apart from reality over time.

The cooling deformation sometimes was misleading with respect to the perceived direction.

While one person during a pilot test stated that she was not able to perceive the actuators 'correction movement' which was performed during the *equilibrium phase*, it showed to cause confusion during the preliminary study. Similar as to our technical evaluation (Figure 6.6) the relative coarse movements could sometimes barely reach the target point. The comparable large correction movement, consequently lead a stronger perceived sensation. This happened most often for movements from the top-left to the top-right and added to the confusion.

As suspected, two participants (P1 and P4) tried to count the number of distinct movements in order to identify the correct shapes. Both, especially tried to deduce the S-SHAPE in this manner. However, only P4 one time could derive the

S-SHAPE successfully by counting ('This time I felt many lines.'). P4 furthermore reported that she sometimes did not choose the same shape as answer again, as she thought it would be unlikely to have the same shape multiple times in a row.

Despite P5 claimed slow gestures to be more noticeable during the session, she also stated to have felt more confident regarding fast gestures after the session. Indeed, most users showed to be more confident regarding fast gestures. However, slow gestures were recognized correctly more than twice as often compared to fast ones. By only looking at the mean noticeability values of *correctly* identified gestures, the fast gestures ($M = 3.5$) also showed to be rated slightly more noticeable compared to slow ones ($M = 2.89$). A possible explanation may be that fast gestures are potentially better perceived and cause a stronger sensation, but slow movements provided the users with more time to reconstruct shapes as described before or exclude others. Although P5 did only select 3 of 15 shapes correctly, she appeared to be good in identifying different speed levels compared to other participants. While the users were not told that the speed may vary within a single gesture, P5 even stated that the speed varied in two cases 'Previous movements were hard to feel because they seemed to be very slow.'. Also 'last two were more noticable' (P5) for the sped up S-SHAPE indicate that faster movements may be more noticeable.

Some users showed to be able to identify a speed change. Regarding the speed level, the user's confidence and number of correct answers revealed a discrepancy.

6.2.7 Conclusion

The prototype clearly showed to still suffer from its low wearability due to the rigid frame which did not align to the curved body features. The tactor appeared to only apply slight pressure. Instead of dragging the skin, it showed to primarily cause motion stimuli. We believe that this issue was mostly introduced through the low wearability, as well as the low friction caused by the tactor in general. As skin stretch stimuli is most critical to directional discriminability [Olausson et al. 2000], we presume that altering the tactor and increasing wearability may therefore drasti-

The low pressure of the tactor showed to result in almost no skin stretch stimuli – making it hard to perceive the direction.

cally increase the noticeability, recognition rate and overall robustness of the gesture perception.

The speed level appeared to influence the perceived sensations.

Despite the low perceptibility of the skin-drag display, the speed level showed to affect the confidence and number of correct answers. Although slow performed gestures were selected correctly more often, fast movements may have resulted in stronger perceived sensations and higher confidence. While our preliminary study does not allow to draw further conclusions, the discrepancy between the confidence and number of correctly perceived shapes regarding the different speed levels appears to be an interesting point to further investigate on in future.

Diagonal lines appeared to increase complexity. However, shapes including diagonals were rated with a slightly higher noticeability and confidence regarding correct shapes. As the diagonal lines of the MIRRORED-Z and the X-SHAPE were slightly longer, users may have perceived the stimuli more easily.

Finally, the cool down time clearly showed to depict a major problem which increased the difficulty of detecting the direction for sequences of movements. The combination of high cool down time and low perceptibility appeared to increase the overall cognitive load of the users in general.

6.3 Design Tool Usability

To gain a first impression about the usability of our design tool we asked the participants from the prior perception study to design several shapes and rate our developed tool regarding different criteria.

6.3.1 Setup

During this study the skin-drag display was connected to a computer via serial port and fixed on a table next to a monitor (30-inch Apple Cinema HD Display, 2560×1600 pixels).

The users sat in front of the table and could program and test the skin-drag display using the developed design tool. The skin-drag display was recorded on video similar to the perception study. In addition, the screen was recorded during the whole session along with the users voice.

6.3.2 Design and Procedure

Users were asked to design and test four shapes with different tasks/requirements.

At the beginning the tool was demoed for the participants by showing them how to program and plot a gesture. They were briefly introduced to the different components in the UI.

The study was divided in four sessions. Within each session the users were asked to design one of four shapes (SQUARE, TRIANGLE, X-SHAPE and Z-SHAPE). For each session they were furthermore given a certain design requirement as task (T1-T4).

- T1: Program the gesture at highest speed.
- T2: Equalize the movement speeds (excluding shadow movements).
- T3: Set the total time to X + 10 sec.
- T4: Design one part of the gesture faster than the other (excluding shadow movements).

A session started after the shape and the design requirement were shown to the participants. The session ended when the participants had programmed the skin-drag display and were satisfied with its state. The sessions, i.e., shapes, were counterbalanced using a Latin Square. The design requirements were applied to the session in the prescribed order.

The users the overall usability, the clarity of specific UI components and the shape matching.

The users were asked to talk aloud throughout the session and informed that questions may only be answered after a session. After each session the users were supposed to rate the design tool and the shape matching with respect to the

the session on a 5-point Likert scale (1 very hard/low - 5 very easy/high). The participants were furthermore asked to state if they encountered a specific challenge, if certain parts of a gesture were perceived to be performed especially bad by the device and if anything may be improved. The users could only visually perceive the state of the skin-drag display.

At the end the users had to fill a questionnaire regarding the overall perceived usability and clarity of the individual UI elements. The questionnaires can be found in Appendix E.

6.3.3 Results and Observations

Novice users showed to quickly get along with the design tool and be able to design gestures. The overall usability was rated to be very high.

The users rated the design tool to be easy to use (Mdn=4) and showed to be very satisfied regarding the tool (Mdn=5) in general. The usability with respect to the individual shapes and tasks turned out to be rated very high (Mdn=5). Only one participant (P1) rated the design tool to be hard to use when he had to design the triangle shape. This was due to the fact that he had to design the first 'closed' shape. When designing closed shapes most users reported difficulties, and asked for a feature to snap/connect the next movement to one of the existing point. This feature had not been implemented. When clicking on an existing point, the movement to the endpoint was selected without creating a new movement. Users had to add a new endpoint somewhere else (either by clicking the '+' icon or inside the view space) and dragging it to the desired target point. Alternatively they could enter the position numerically. However, the numerical input field for the position was rarely touched.

Shape Matching

When it comes to the matching of the designed gesture and the performed result of the actuator, the system was rated with a median value of 4 on a 5-point Likert scale (1 not matching at all - 5 perfectly matching). The triangle was rated to be less matching (Mdn=3) compared to the others

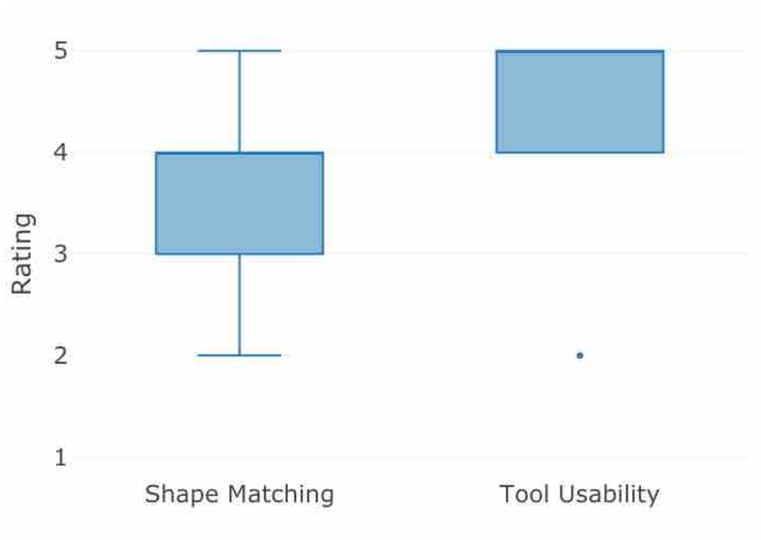

Figure 6.12: Overall shape matching and usability ratings on a 5-point Likert scale (1 very low - 5 very high).

(Mdn=4). The diagonals of which the triangle was composed showed to be most critical for the actuator movements when sped down.

Several users reported to spot curvy movements caused by the cooling deformation. The overall shape matching was still rated to be high.

Several subjects reported that some '[...] lines were more like curves.' (P1,P4). Similar to what had already been observed within the gesture recognition task, a correction during the *equilibrium phase* resulted in a 'speed up' at the end of long and slow movements. This was also noticed by the users 'There was a speed difference during slow movements.' (P1). Despite P4 was being aware of the *shadow movement* concept, she tried to design shapes without any *shadow movements* by only making use of one quarter of the EMA in two cases (Z-SHAPE and SQUARE).

UI Components

The overall clarity of the individual UI components was rated to be very clear (Mdn=5). Some participants suggested adding the speed and shadow movement to the table view. A more frequently asked feature was to allow

The overall clarity was rated to be very high. Frequently asked features mainly comprised ones known from common vector graphics and spreadsheet tools.

to add movements not only at the end, but in-between the individual movement paths, e.g. 'by clicking on existing movement lines' (P4). Several participants had also been looking for a feature which allows to set the speed and movement times for multiple movements at once. P3 asked for an additional button, P4 recommended allowing multi-selection in this case.

6.3.4 Conclusion

The usability study showed that novice users are able to easily design gestures and the participants were already highly satisfied with the developed tool. The most frequently requested features appeared to come from prior experience with vector graphics and spreadsheet applications. The most challenging part during the design of gestures unveiled to be closing a shape, i.e. connecting the start and end point. A snapping feature could simplify this task in future.

Chapter 7

Summary and future work

7.1 Summary and contributions

This thesis aimed to investigate on the feasibility of a programmable and unobtrusive wearable interface which takes advantage of SMA actuators in order to replay two-dimensional skin-drag gestures.

We therefore first looked into different design and implementation concepts of SMA actuators (chapter 3). We investigated on how one can gain control about the actuation of a single SMA spring and discussed the advantages as well as disadvantages of different actuator configurations. Within a first test we saw that one can increase the *contraction frequency* of spring actuators by using a second SMA as *active bias force* in place of a conventional mechanical spring. In a second test we investigated on the feasibility of a feedback loop by sensing the resistance of an SMA spring actuator. We concluded that measuring the resistance does not provide a reliable reference value in our case. Next to simple implementation and control techniques for SMA spring actuators, we described how more advanced topologies can be realized and proposed a general method to control them. We furthermore presented a generic controller board which puts our proposed method into practice. Although we encountered some bottlenecks, the controller board provided the essential functionality and allowed us to demonstrate how small a control unit could possibly get.

Based on the gathered experience described in chapter 3, we presented a first proof-of-concept of a thin and soft skin-drag display which uses a star topology of four antagonistic SMA spring actuators in order to move a tactor across the skin (chapter 4). We explained our design decisions and showed how the different design parameters can be determined. In addition, we described how we developed our control model and discussed the underlying assumptions along with the resulting trade-offs. We built a control system which drives the SMA actuators according to our control model without the need of an external feedback system. Finally, we created a design tool which aims to allow researchers to program our skin-drag display and explore diverse gestures in an easy way (chapter 5).

We evaluated our proposed system in several ways regarding the robustness of our control model, the accuracy and consistency of our device, gesture perception and design tool usability (chapter 6). Our technical evaluation revealed that our high-level assumptions for the control model already allow for a robust control of the spring actuators. Despite our device exhibited a systematic error which correlates with the distance to the center, we found that our system is able to perform skin-drag gestures very consistently. In contrast to our pilot tests, our preliminary user study showed that users still have problems to recognize different gestures. We concluded that this was mainly due to the the low wearability of our planar frame as we observed that the tactor was applying low pressure. We believe that this lead to a low perceptibility of the direction of a movement. In addition, the long cool down appeared to have added to the mental load. The results of our usability study let suggest that our design tool provides an intuitive user interface which allows novice users to program our skin-drag display in an easy way.

7.2 Limitations and Future Work

7.2.1 Skin-drag Display

In future, we aim to conduct a user study which investigates on the perceptibility when using our flexible frame. We believe that the flexible frame would already increase the perceptibility of the replayed skin-drag gestures significantly, as the tactor would apply more pressure and produce a stronger skin-stretch stimulus. Our preliminary has shown that the users noticed that the tactor was moving but had a hard time to tell the direction. Olausson et al. suggest that skin-stretch is a critical factor in order to perceive the direction of a moving stimulus. Thus, we furthermore aim to test different types of tactors to increase the friction and investigate on how different form factors and matters influence the skin-drag sensation.

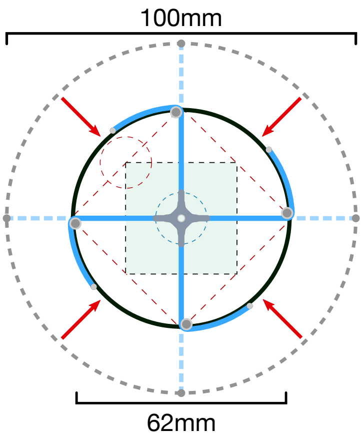

Figure 7.1: By redirecting the contraction force of the SMAs (blue) using pulleys (gray), the system's diameter can be decreased from $100mm$ (dashed line) to approximately $62mm$ (black line).

Another important step towards improving the wearability depicts shrinking the overall size of our device. Despite the prototype already unveils to be relatively flat (3-$4mm$ thickness), the diameter of the circular frame ($100mm$) still shows to be very large compared with the estimated workspace area of $32.16mm \times 32.16mm$. A smaller frame would allow to test the device at more common body locations to provide haptic feedback, such as the forearm. Figure 7.1 illustrates how pulleys could help to shrink the system diameter from $100mm$ to $62mm$ and thereby increases the effectively used space.

We moreover assume that a future extension could replace our *shadow movement* concept by implementing a controllable tactor which only applies pressure if wanted. To do so, e.g. a mechanical spring and an additional SMA could be used to pull down the tactor and produce the desired tactile sensation at the right moment. To prevent potentially bent SMA springs from causing unintended and imbalanced pressure, we propose that some sort of gliding plate could be introduced which distributes the pressure as indicated in Figure 7.2. A controllable tactor could this way still produce pointed sensations on curved body surfaces while the gliding plate causes a comparably weak sensation. By doing so the the device could support a much larger variety of possible gestures and therefore reach a higher degree of expressiveness.

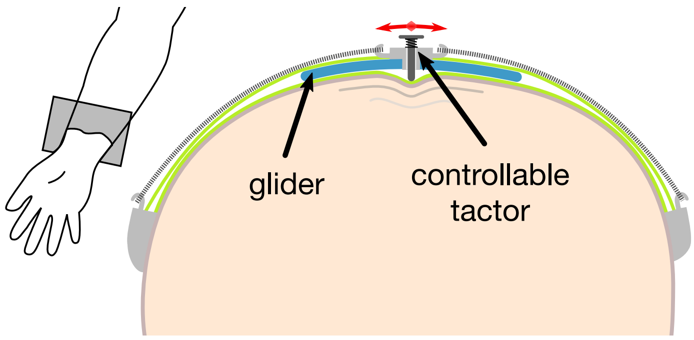

Figure 7.2: A glider moves along with the tactor across the skin resulting in distributed pressure introduced by the bend springs. A controlled tactor only applies pointed tactile sensations if wanted.

7.2.2 Control Unit

Another critical factor to the perceptibility and expressiveness of our device revealed to be the comparable long *cooling phase* of our control model. Within our perception study we could observe, that the constant amount of time after each movement added to the mental load of the participants. We also saw that during the cool down the cooling deformation impacts the shape matching. While we believe that a higher friction and a stronger sensation would already lower the impact of the *cooling phase* it is preferably minimized in order to replay gestures more fluently and faster.

To decrease the cool down time we suggest adding active cooling by using Peltier elements or simply implementing a liquid which increases the thermal conductivity and thereby accelerates the heat transfer. The control system could furthermore try to model the thermal effects or take advantage of a feedback system. Being able to roughly model the occurring effects could already allow to perform more fluent gestures. The user interface may inform the designer to which degree the speed or effective movement area decreases when lowering the cooldown time.

Regardless of the *cooling phase*, our control model is still limited to straight movements. Future work could extend the proposed system by allowing to perform circular movements. Finally the systematic error that has been identified within our technical evaluation should be incorporated into the control model in order to increase the overall accuracy for targets closer to the border.

Appendix A

Generic Spring Controller Board Schematic

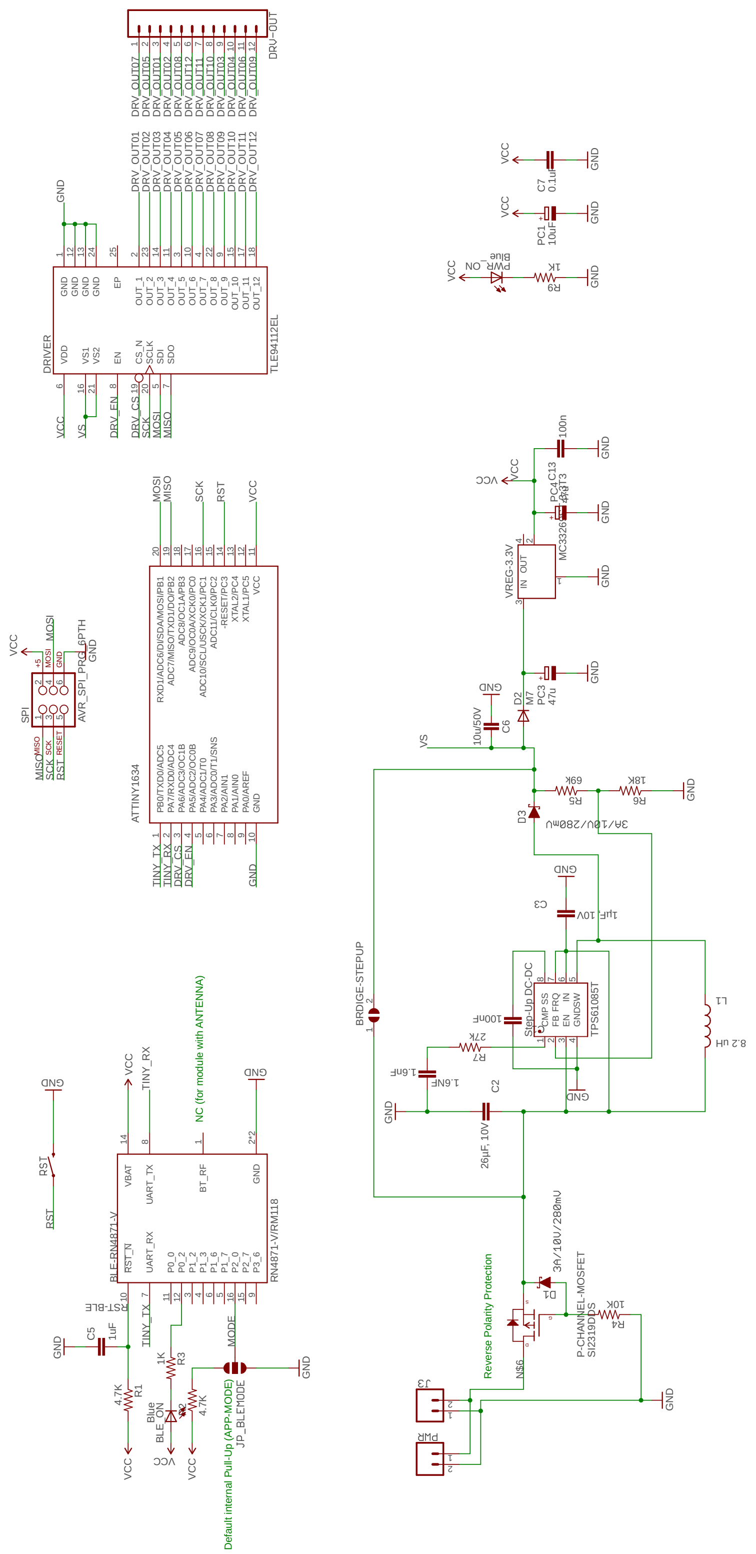

Figure A.1: Generic Spring Controller Board Schematic

Appendix B

Skin-drag Display Control Circuit Schematic

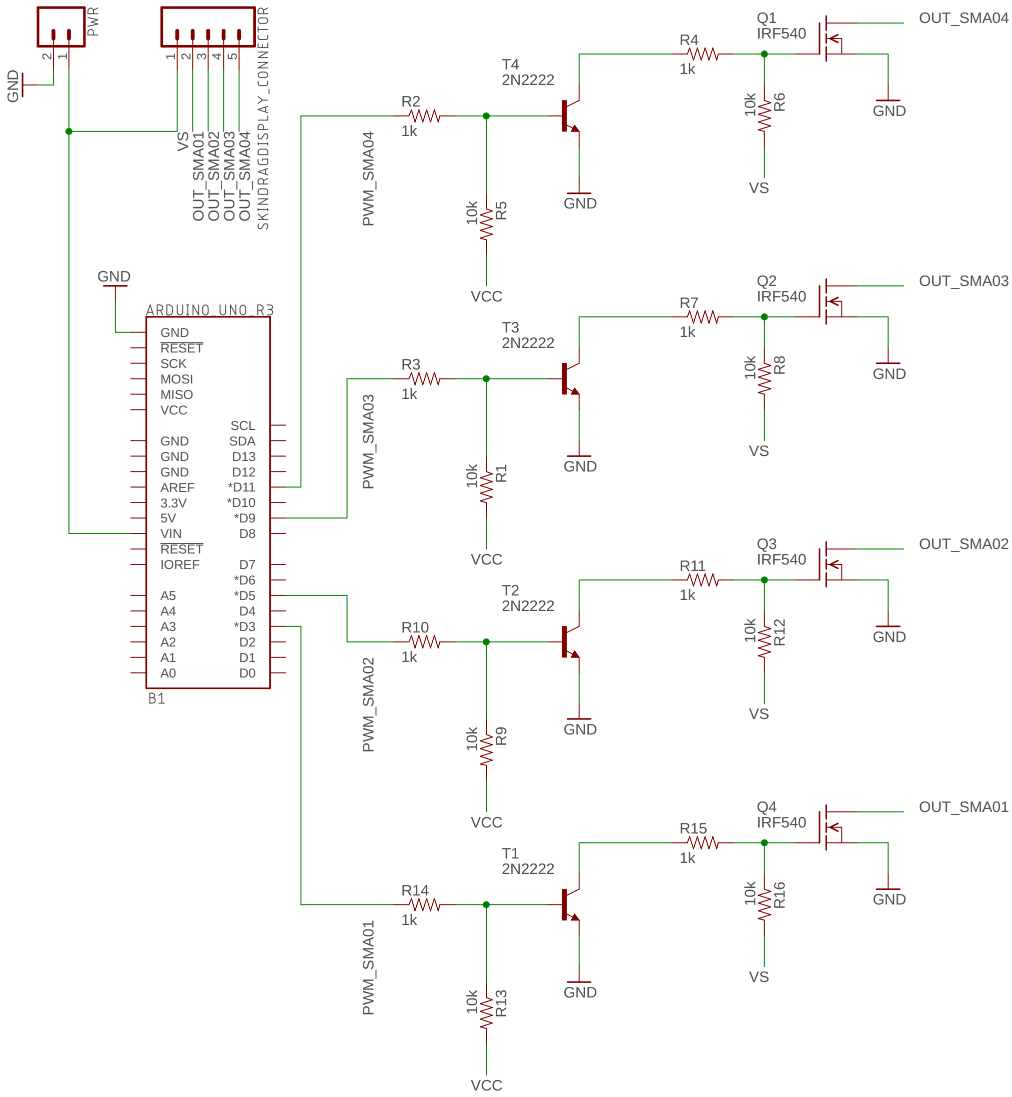

Figure B.1: Skin-drag Display Control Circuit Schematic

Appendix C

Time-Distance-Power Relation

$$T_p(d) = t(d^{g(p)})^{h(p)}$$

$$g(p) = 0.9988849 + \frac{1.288355 - 0.9988849}{1 + (\frac{p}{12.14066})^{4.240305}}$$
$$h(p) = 0.8391275 + \frac{1.347852 - 0.8391275}{1 + (\frac{p}{25.38628})^{1.347124}}$$

$$t(x) = \begin{cases} s_1(x) & 0 \leq x < 0.055 \\ s_2(x) & 0.055 \leq x < 21.11508198 \\ s_3(x) & 21.11508198 \leq x \end{cases}$$

$$\begin{aligned}
s_1(x) &= 888.2373305127733x - 4847.53939592249x^3 \\
s_2(x) &= 24.582586475803367 + 430.77799730142283x \\
&\quad - 146.00670875668141x^2 + 33.139768599012676x^3 \\
&\quad - 4.5191835604370194x^4 + 0.36629490380189034x^5 \\
&\quad - 0.017246792614173400x^6 + 0.00043539390155004394x^7 \\
&\quad - 0.0000045548864384476225x^8 \\
s_3(x) &= 88838823.979520223627 - 8212.1883029048913x \\
&\quad + 646.85479089192700x^2 - 22.057526175511740x^3 \\
&\quad + 0.27784732477792562x^4
\end{aligned}$$

Appendix D

Perception Study Questionnaires

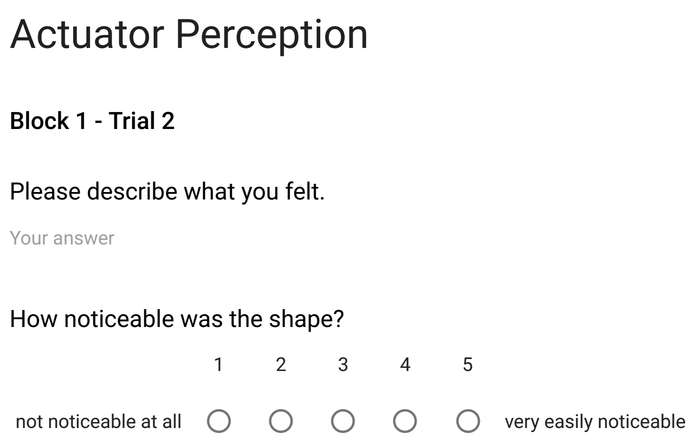
Actuator Perception

Block 1 - Trial 2

Please describe what you felt.

Your answer

How noticeable was the shape?

	1	2	3	4	5	
not noticeable at all	○	○	○	○	○	very easily noticeable

Figure D.1: Perception Study Questionnaire Trials (1)

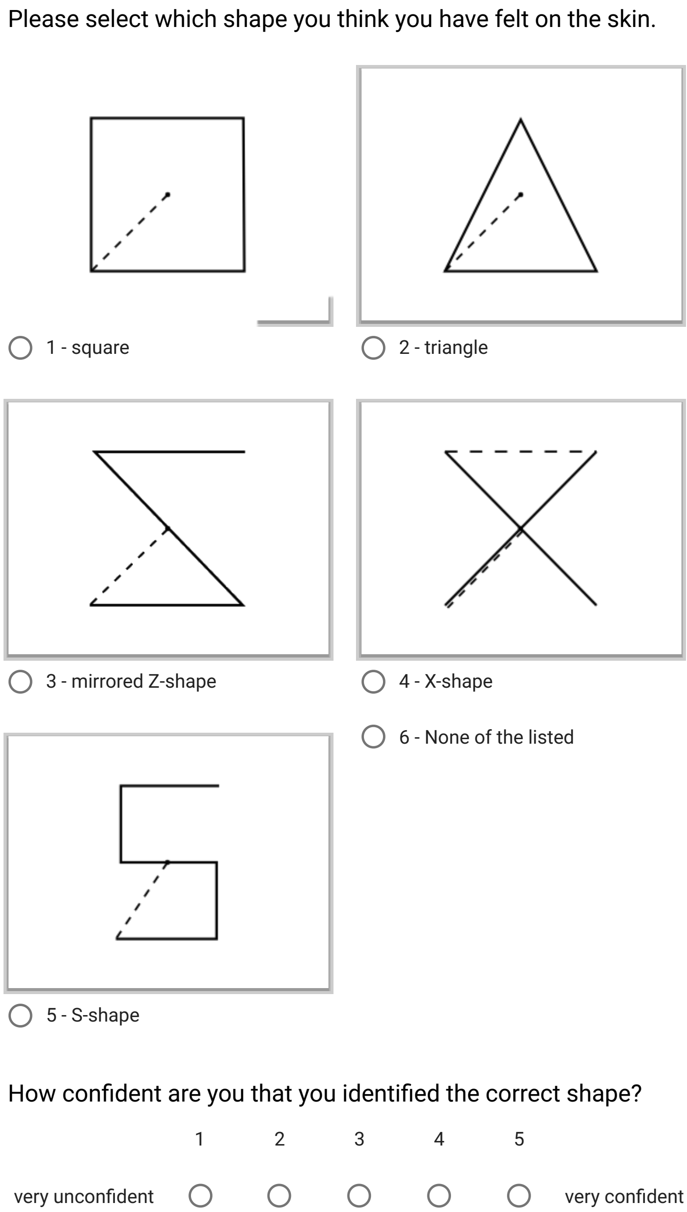

Please select which shape you think you have felt on the skin.

1 - square

2 - triangle

3 - mirrored Z-shape

4 - X-shape

6 - None of the listed

5 - S-shape

How confident are you that you identified the correct shape?

	1	2	3	4	5	
very unconfident	○	○	○	○	○	very confident

Figure D.2: Perception Study Questionnaire Trials (2)

How fast was the speed compared to the trial before?

- ○ slower
- ○ faster
- ○ equal

How comfortable did the shape feel?

	1	2	3	4	5	
very uncomfortable	○	○	○	○	○	very comfortable

Figure D.3: Perception Study Questionnaire Trials (3)

Actuator Perception

Overall

How noticeable was the actuator on average?

	1	2	3	4	5	
not noticeable at all	○	○	○	○	○	very easily not

How comfortable was the actuator on average?

	1	2	3	4	5	
very uncomfortable	○	○	○	○	○	very comfortable

How distinguishable were the shapes between the blocks?

	1	2	3	4	5	
they all felt the same	○	○	○	○	○	very well distinguishable

Did you find some shapes be more distinguishable than others? If so, please describe which and why.

Your answer

How well could you feel when a shape was slowed down or sped up?

	1	2	3	4	5	
very bad	○	○	○	○	○	very well

Did shape speed influence perception? If so, how?

Your answer

Did shape speed influence distinction? If so, how?

Your answer

Did shape speed influence comfort? If so, how?

Your answer

Figure D.4: Perception Study Questionnaire Trials

Appendix E

Usability Study Questionnaires

Tool Usability

Session 1

Describe how easy the tool felt to use for the given task.

	1	2	3	4	5	
very hard to use	○	○	○	○	○	very easy to use

What UI elements were challenging to understand?

Your answer

How far did the physical result match the programmed design?

	1	2	3	4	5	
did not match at all	○	○	○	○	○	matched perfectly

If the result did not match your design, please explain what did not match most.

Your answer

What do you think that might be improved if the programming of the design tool is done again?

Your answer

Figure E.1: Usability Study Questionnaire Trials

Tool Usability

Overall

On average, how easy was the tool to use?

	1	2	3	4	5	
very hard to use	○	○	○	○	○	very easy to use

How would you rate the clarity of the individual UI elements?

	very unclear	unclear	neutral	clear	very clear
movement area view	○	○	○	○	○
view options	○	○	○	○	○
movement list	○	○	○	○	○
position input fields	○	○	○	○	○
cooldown time	○	○	○	○	○
movement time	○	○	○	○	○
speed	○	○	○	○	○
total time	○	○	○	○	○

Which main challenges did you face, if any?

Your answer

Please rate your overall satisfaction with the tool.

	1	2	3	4	5	
not satisfied at all	○	○	○	○	○	very satisfied

Do you have any other comments or recommendations?

Your answer

Figure E.2: Usability Study Questionnaire Overall

Bibliography

Feier Cao, MHD Yamen Saraiji, and Kouta Minamizawa. 2018. Skin+. In *ACM SIGGRAPH 2018 Posters on - SIGGRAPH '18*. ACM Press, New York, New York, USA, 1–2. https://doi.org/10.1145/3230744.3230772

Nathaniel A. Caswell, Ryan T. Yardley, Markus N. Montandon, and William R. Provancher. 2012. Design of a forearm-mounted directional skin stretch device. In *2012 IEEE Haptics Symposium (HAPTICS)*. IEEE, 365–370. https://doi.org/10.1109/HAPTIC.2012.6183816

J. Cederström and J. Van Humbeeck. 1995. Relationship Between Shape Memory Material Properties and Applications. *Le Journal de Physique IV* 05, C2 (2 1995), 2–335. https://doi.org/10.1051/jp4:1995251

Hiroki Cho, Takaei Yamamato, Yuji Takeda, Akihiko Suzuki, and Toshio Sakuma. 2010. Exploitation of shape memory alloy actuator using resistance feedback control and its development. *Progress in Natural Science: Materials International* 20, 1 (2010), 97–103. https://doi.org/10.1016/S1002-0071(12)60013-6

Jean-Baptiste Chossat, Daniel K. Y. Chen, Yong-Lae Park, and Peter B. Shull. 2019. Soft Wearable Skin-Stretch Device for Haptic Feedback using Twisted and Coiled Polymer Actuators. *IEEE Transactions on Haptics* PP, c (2019), 1–1. https://doi.org/10.1109/TOH.2019.2943154

Marcelo Coelho, Hiroshi Ishii, and Pattie Maes. 2008. Surflex. In *Proceeding of the twenty-sixth annual CHI conference extended abstracts on Human factors in computing systems -*

CHI '08. ACM Press, New York, New York, USA, 3429. https://doi.org/10.1145/1358628.1358869

Marcelo Coelho and Pattie Maes. 2008. Sprout I/O. In *Proceedings of the 2nd international conference on Tangible and embedded interaction - TEI '08*. ACM Press, New York, New York, USA, 221. https://doi.org/10.1145/1347390.1347440

Patrick Delmas, Jizhe Hao, and Lise Rodat-Despoix. 2011. Molecular mechanisms of mechanotransduction in mammalian sensory neurons. *Nature Reviews Neuroscience* 12, 3 (3 2011), 139–153. https://doi.org/10.1038/nrn2993

Julia C. Duvall, Nicholas Schleif, Lucy E. Dunne, and Brad Holschuh. 2016. Active "hugging" vest for deep touch pressure therapy. *UbiComp 2016 Adjunct - Proceedings of the 2016 ACM International Joint Conference on Pervasive and Ubiquitous Computing* (2016), 458–463. https://doi.org/10.1145/2968219.2971344

DYNALLOY Inc. 2019. FLEXINOL® Actuator Spring Technical and Design Data. (2019). https://www.dynalloy.com/tech_data_springs.php

B. B. Edin. 1992. Quantitative analysis of static strain sensitivity in human mechanoreceptors from hairy skin. *Journal of Neurophysiology* (1992). https://doi.org/10.1152/jn.1992.67.5.1105

Stephen J. Furst, John H. Crews, and Stefan Seelecke. 2013. Stress, strain, and resistance behavior of two opposing shape memory alloy actuator wires for resistance-based self-sensing applications. *Journal of Intelligent Material Systems and Structures* 24, 16 (11 2013), 1951–1968. https://doi.org/10.1177/1045389X13486715

Frank A. Geldard. 1960. Some Neglected Possibilities of Communication. *Science* 131, 3413 (5 1960), 1583–1588. https://doi.org/10.1126/science.131.3413.1583

Jun Gong, Da Yuan Huang, Teddy Seyed, Te Lin, Tao Hou, Xin Liu, Molin Yang, Boyu Yang, Yuhan Zhang, and

Xing Dong Yang. 2018. Jetto: Using lateral force feedback for smartwatch interactions. In *Conference on Human Factors in Computing Systems - Proceedings*, Vol. 2018-April. ACM Press, New York, New York, USA, 1–14. https://doi.org/10.1145/3173574.3174000

J. A B Gray and P. B C Matthews. 1951. A comparison of the adaptation of the Pacinian corpuscle with the accommodation of its own axon. *The Journal of Physiology* 114, 4 (8 1951), 454–464. https://doi.org/10.1113/jphysiol.1951.sp004636

Aakar Gupta, Antony Albert Raj Irudayaraj, and Ravin Balakrishnan. 2017. HapticClench: Investigating squeeze sensations using memory alloys. In *UIST 2017 - Proceedings of the 30th Annual ACM Symposium on User Interface Software and Technology*. ACM Press, New York, New York, USA, 109–117. https://doi.org/10.1145/3126594.3126598

Nur Al-huda Hamdan, Adrian Wagner, Simon Voelker, Jürgen Steimle, and Jan Borchers. 2019. Springlets. In *Proceedings of the 2019 CHI Conference on Human Factors in Computing Systems - CHI '19*. ACM Press, New York, New York, USA, 1–14. https://doi.org/10.1145/3290605.3300718

Teng Han, Fraser Anderson, Pourang Irani, and Tovi Grossman. 2018. Hydroring: Supporting mixed reality haptics using liquid flow. In *UIST 2018 - Proceedings of the 31st Annual ACM Symposium on User Interface Software and Technology*. ACM Press, New York, New York, USA, 913–925. https://doi.org/10.1145/3242587.3242667

Liang He, Cheng Xu, Ding Xu, and Ryan Brill. 2015. Pneuhaptic: Delivering haptic cues with a pneumatic armband. In *ISWC 2015 - Proceedings of the 2015 ACM International Symposium on Wearable Computers*. 47–48. https://doi.org/10.1145/2802083.2802091

Alexandra Ion, Edward Wang, and Patrick Baudisch. 2015. Skin drag displays: Dragging a physical tactor across the user's skin produces a stronger tactile stimulus than vibrotactile. In *Conference on Human Factors in Computing*

Systems - Proceedings, Vol. 2015-April. ACM Press, New York, New York, USA, 2501–2504. https://doi.org/10.1145/2702123.2702459

Seungwoo Je, Brendan Rooney, Liwei Chan, and Andrea Bianchi. 2017. tactoRing: A skin-drag discrete display. In *Conference on Human Factors in Computing Systems - Proceedings*, Vol. 2017-May. ACM Press, New York, New York, USA, 3106–3114. https://doi.org/10.1145/3025453.3025703

Yeon Sub Jin, Han Yong Chun, Eun Tai Kim, and Sungchul Kang. 2014. VT-ware: A wearable tactile device for upper extremity motion guidance. In *IEEE RO-MAN 2014 - 23rd IEEE International Symposium on Robot and Human Interactive Communication: Human-Robot Co-Existence: Adaptive Interfaces and Systems for Daily Life, Therapy, Assistance and Socially Engaging Interactions*. IEEE, 335–340. https://doi.org/10.1109/ROMAN.2014.6926275

D. Josephine Selvarani Ruth, S. Sunjai Nakshatharan, and D. Dhanalakshmi. 2014. Differential resistance feedback control of a self-sensing shape memory alloy actuated system. *ISA Transactions* 53, 2 (2014), 289–297. https://doi.org/10.1016/j.isatra.2013.11.002

Seung Chan Kim, Chong Hui Kim, Gi Hun Yang, Tae Heon Yang, Byung Kil Han, Sung Chul Kang, and Dong Soo Kwon. 2009. Small and Lightweight Tactile Display(SaLT) and Its Application. In *Proceedings - 3rd Joint EuroHaptics Conference and Symposium on Haptic Interfaces for Virtual Environment and Teleoperator Systems, World Haptics 2009*. IEEE, 69–74. https://doi.org/10.1109/WHC.2009.4810820

Espen Knoop and Jonathan Rossiter. 2015. The Tickler. In *Proceedings of the 33rd Annual ACM Conference Extended Abstracts on Human Factors in Computing Systems - CHI EA '15*, Vol. 18. ACM Press, New York, New York, USA, 1133–1138. https://doi.org/10.1145/2702613.2732749

Efthymios Kolyvas and Anthony Tzes. 2018. Model based design of antagonistic shape memory alloy spring devices. *Journal of Intelligent Material Systems and Struc-*

tures 29, 12 (7 2018), 2619–2640. https://doi.org/10.1177/1045389X18770880

Ig Mo Koo, Kwangmok Jung, Ja Choon Koo, Jae Do Nam, Young Kwan Lee, and Hyouk Ryeol Choi. 2008. Development of soft-actuator-based wearable tactile display. *IEEE Transactions on Robotics* 24, 3 (6 2008), 549–558. https://doi.org/10.1109/TRO.2008.921561

Seungyon Claire Lee and Thad Starner. 2009. Mobile gesture interaction using wearable tactile displays. In *Proceedings of the 27th international conference extended abstracts on Human factors in computing systems - CHI EA '09*. ACM Press, New York, New York, USA, 3437. https://doi.org/10.1145/1520340.1520499

N. Lewis, A. York, and S. Seelecke. 2013. Experimental characterization of self-sensing SMA actuators under controlled convective cooling. *Smart Materials and Structures* 22, 9 (9 2013), 094012. https://doi.org/10.1088/0964-1726/22/9/094012

Jason Lin, Jasmine Zhou, and Helen Koo. 2015. Enfold. In *Proceedings of the 2015 ACM International Joint Conference on Pervasive and Ubiquitous Computing and Proceedings of the 2015 ACM International Symposium on Wearable Computers - UbiComp '15*. ACM Press, New York, New York, USA, 563–566. https://doi.org/10.1145/2800835.2801671

Pedro Lopes, Alexandra Ion, and Patrick Baudisch. 2015a. Impacto. In *Proceedings of the 28th Annual ACM Symposium on User Interface Software & Technology - UIST '15*. ACM Press, New York, New York, USA, 11–19. https://doi.org/10.1145/2807442.2807443

Pedro Lopes, Alexandra Ion, and Patrick Baudisch. 2015b. Impacto: Simulating p hysical i mpact by combining tactile stimulation with electrical mu scle stimulation. *UIST 2015 - Proceedings of the 28th Annual ACM Symposium on User Interface Software and Technology* (2015), 11–19. https://doi.org/10.1145/2807442.2807443

Granit Luzhnica and Eduardo Veas. 2019. Optimising Encoding for Vibrotactile Skin Reading. In *Proceedings of the 2019 CHI Conference on Human Factors in Computing*

Systems - CHI '19. ACM Press, New York, New York, USA, 1–14. https://doi.org/10.1145/3290605.3300465

N. Ma, G. Song, and H. J. Lee. 2004. Position control of shape memory alloy actuators with internal electrical resistance feedback using neural networks. *Smart Materials and Structures* 13, 4 (2004), 777–783. https://doi.org/10.1088/0964-1726/13/4/015

Jess Mcintosh, Paul Strohmeier, Jarrod Knibbe, Sebastian Boring, and Kasper Hornbæk. 2019. Magnetips: Combining fingertip tracking and haptic feedback for around-device interaction. In *Conference on Human Factors in Computing Systems - Proceedings*. ACM Press, New York, New York, USA, 1–12. https://doi.org/10.1145/3290605.3300638

Jaronie Mohd Jani, Martin Leary, Aleksandar Subic, and Mark A. Gibson. 2014. A review of shape memory alloy research, applications and opportunities. (4 2014), 1078–1113 pages. https://doi.org/10.1016/j.matdes.2013.11.084

Paul Motzki. 2018. *Advanced Design and Control Concepts for Actuators Based on Shape Memory Alloy Wires*. Ph.D. Dissertation. Saarland University. https://doi.org/10.22028/D291-27354

Akira Nakayasu. 2016. Luminescent tentacles. In *SIGGRAPH ASIA 2016 Art Gallery on - SA '16*. ACM Press, New York, New York, USA, 1–1. https://doi.org/10.1145/3004257.3004486

Takuya Nojima, Yoshiharu Ooide, and Hiroki Kawaguchi. 2013. Hairlytop interface: An interactive surface display comprised of hair-like soft actuators. In *2013 World Haptics Conference (WHC)*. IEEE, 431–435. https://doi.org/10.1109/WHC.2013.6548447

Håkan Olausson. 1994. The influence of spatial summation on human tactile directional sensibility. *Somatosensory & Motor Research* 11, 4 (1 1994), 305–310. https://doi.org/10.3109/08990229409028874

Håkan Olausson, Imad Hamadeh, Parham Pakdel, and Ulf Norrsell. 1998. Remarkable capacity for perception of the direction of skin pull in man. *Brain Research* 808, 1 (10 1998), 120–123. https://doi.org/10.1016/S0006-8993(98)00838-5

Håkan Olausson, Johan Wessberg, and Naoyuki Kakuda. 2000. Tactile directional sensibility: peripheral neural mechanisms in man. *Brain Research* 866, 1-2 (6 2000), 178–187. https://doi.org/10.1016/S0006-8993(00)02278-2

Yoshiharu Ooide, Hiroki Kawaguchi, and Takuya Nojima. 2013. An assembly of soft actuators for an organic user interface. In *Proceedings of the adjunct publication of the 26th annual ACM symposium on User interface software and technology - UIST '13 Adjunct*. ACM Press, New York, New York, USA, 87–88. https://doi.org/10.1145/2508468.2514723

Young-Woo Park, Joohee Park, and Tek-Jin Nam. 2015. The Trial of Bendi in a Coffeehouse. In *Proceedings of the 33rd Annual ACM Conference on Human Factors in Computing Systems - CHI '15*, Vol. 2015-April. ACM Press, New York, New York, USA, 2181–2190. https://doi.org/10.1145/2702123.2702326

Fabrizio Pece, Juan Jose Zarate, Velko Vechev, Nadine Besse, Olexandr Gudozhnik, Herbert Shea, and Otmar Hilliges. 2017. MagTics: Flexible and thin form factor magnetic actuators for dynamic and wearable haptic feedback. In *UIST 2017 - Proceedings of the 30th Annual ACM Symposium on User Interface Software and Technology*. 143–154. https://doi.org/10.1145/3126594.3126609

Kathrin Probst, Thomas Seifried, Michael Haller, Kentaro Yasu, Maki Sugimoto, and Masahiko Inami. 2011. Move-it. In *Proceedings of the 2011 annual conference extended abstracts on Human factors in computing systems - CHI EA '11*. ACM Press, New York, New York, USA, 1393. https://doi.org/10.1145/1979742.1979780

Isabel P. S. Qamar, Rainer Groh, David Holman, and Anne Roudaut. 2018. HCI meets Material Science. In *Proceedings of the 2018 CHI Conference on Human Factors in*

Computing Systems - CHI '18. ACM Press, New York, New York, USA, 1–23. https://doi.org/10.1145/3173574.3173948

M. Sato. 1961. Response of Pacinian corpuscles to sinusoidal vibration. *The Journal of Physiology* 159, 3 (12 1961), 391–409. https://doi.org/10.1113/jphysiol.1961.sp006817

Robert Scheibe, Mathias Moehring, and Bernd Froehlich. 2007. Tactile Feedback at the Finger Tips for Improved Direct Interaction in Immersive Environments. In *2007 IEEE Symposium on 3D User Interfaces*. IEEE, 123–130. https://doi.org/10.1109/3DUI.2007.340784

Massimiliano Solazzi, William R. Provancher, Antonio Frisoli, and Massimo Bergamasco. 2011. Design of a SMA actuated 2-DoF tactile device for displaying tangential skin displacement. In *2011 IEEE World Haptics Conference*. IEEE, 31–36. https://doi.org/10.1109/WHC.2011.5945457

Daniel Spelmezan, Rafael Morales González, and Sriram Subramanian. 2016. SkinHaptics: Ultrasound focused in the hand creates tactile sensations. *IEEE Haptics Symposium, HAPTICS* 2016-April (2016), 98–105. https://doi.org/10.1109/HAPTICS.2016.7463162

Andrew A. Stanley and Katherine J. Kuchenbecker. 2011. Design of body-grounded tactile actuators for playback of human physical contact. In *2011 IEEE World Haptics Conference*. IEEE, 563–568. https://doi.org/10.1109/whc.2011.5945547

Evan Strasnick, Jessica R Cauchard, and James A Landay. 2017. BrushTouch. In *Proceedings of the 2017 CHI Conference on Human Factors in Computing Systems - CHI '17*, Vol. 2017-May. ACM Press, New York, New York, USA, 3120–3125. https://doi.org/10.1145/3025453.3025759

L. Sun, W.M. Huang, Z. Ding, Y. Zhao, C.C. Wang, H. Purnawali, and C. Tang. 2012. Stimulus-responsive shape memory materials: A review. *Materials & Design* 33 (1 2012), 577–640. https://doi.org/10.1016/j.matdes.2011.04.065

Hong Z. Tan and Alex Pentland. 1997. Tactual displays for wearable computing. In *International Symposium on Wearable Computers, Digest of Papers*. IEEE Comp Soc, 84–89. https://doi.org/10.1007/BF01682025

TOKI Corporation. 2017. BioMetal Helix Actuators (BMX Catalog). (2017). https://www.toki.co.jp/biometal/download/downloadfiles/BMX_Catalog_140217.pdf

Hsin-Ruey Tsai, Jun Rekimoto, and Bing-Yu Chen. 2019. ElasticVR. In *Proceedings of the 2019 CHI Conference on Human Factors in Computing Systems - CHI '19*. ACM Press, New York, New York, USA, 1–10. https://doi.org/10.1145/3290605.3300450

Tian Miao Wang, Zhen Yun Shi, Da Liu, Chen Ma, and Zhen Hua Zhang. 2012. An accurately controlled antagonistic shape memory alloy actuator with self-sensing. *Sensors (Switzerland)* 12, 6 (2012), 7682–7700. https://doi.org/10.3390/s120607682

Anusha Withana, Daniel Groeger, and Jürgen Steimle. 2018. Tacttoo: A thin and feel-through tattoo for on-skin tactile output. In *UIST 2018 - Proceedings of the 31st Annual ACM Symposium on User Interface Software and Technology*. ACM Press, New York, New York, USA, 365–378. https://doi.org/10.1145/3242587.3242645

Acronyms

CNC computer numerical control

DEA dielectric elastomer actuator

EMA effective movement area

FSMA ferromagnetic shape-memory alloy

FEA fluidic elastomer actuator

GUI graphical user interface

HCI human-computer interaction

MDF medium-density fibreboard

NiTi nickel-titanium

PWM pulse-width modulation

SMA shape-memory alloy

SME shape-memory effect

TCP twisted and coiled polymer

TULA tiny ultrasonic linear actuator

VR Virtual Reality

Index

active coils . . . 21
actuation method . . . 17
assembly . . . 49
attachment . . . 35, 49
austenite phase . . . 16

back-end . . . 50
bias force . . . 24
- active vs. passive . . . 25, 26
body grounding . . . 35

calibration phase . . . 46
circuit board . . . 50
command interface . . . 52
common node . . . 32
contracted length . . . 20
contraction force . . . 16
contraction frequency . . . 21, 26
control loop . . . 28
control method
- advanced . . . 32
- basic . . . 23
control model . . . 39–48
- boosted movements model . . . 42
- force equilibrium model . . . 41
- hybrid model . . . 46
- phases . . . 46
control parameters . . . 21
control system . . . 50
control unit . . . 50
controller board . . . 35
cool down . . . 57
cooling phase . . . 47, 57

design material . . . 14
design parameters . . . 20
design tool . . . 55
displacement factor . . . 20

displacement length 20
display
- design 37–39
- implementation 48–50
- parameters 38
duty cycle 24, 51

effective movement area 38
electrical current 21, 51
elongated length 20

feedback loop 28
flexible frame 49
force equilibrium 41
form factor 19
front-end 55
future work 87–89

gate driver 23
gesture design 58
graphical user interface 55

half-bridge 33
heat transfer 18
heating 22
hysteresis 18

Jule effect 17

level shifter 24

machine controller 50, 51
- instructions 52
magnetic SME 15
martensite phase 16
maximum power 51
motion system 39
movement area 55
movement list 55
movement parameters 55
movement path 52, 58
movement settings 55
movement time 59

NiTi SMA 16
non-linear behavior 18

one-way SME 14
open-loop control 40
operation point 25
operational boundaries 21

power supply 51
power value 51
preliminary user study 71–84
PWM signal 23

repeated contractions 24

shadow movement 57
shape-memory alloy 14
shape-memory effect 14–15
skin-drag gesture 51
SMA actuator characteristics 17
SMA contraction 23
SMA resistance 22, 29
SMA spring 19, 20
SMA types 14–15
SMA wire 19
solid length 20
speed control 59
spring parameters 20
stretch ratio 20
summary 85–86
system feedback 53, 60

tactor 48
technical evaluation 61–71
temperature 21
temperature thresholds 17
test
- contraction frequency 26
- self sensing 28
thermal SME 15
time-distance-power relation 43
topologies 30
topology
- chain 30
- connection 31
- mesh 30
- node 31
- star 30
transformation threshold 16
traveling time 52, 59
two-way SME 14

wire diameter 20
workspace 39

Typeset December 19, 2019